

Generative Adversarial User Privacy in Lossy Single-Server Information Retrieval

Chung-Wei Weng, Yauhen Yakimenka, Hsuan-Yin Lin, *Senior Member, IEEE*,
Eirik Rosnes, *Senior Member, IEEE*, and Jörg Kliewer, *Senior Member, IEEE*

Abstract—We propose to extend the concept of private information retrieval by allowing for distortion in the retrieval process and relaxing the perfect privacy requirement at the same time. In particular, we study the trade-off between download rate, distortion, and user privacy leakage, and show that in the limit of large file sizes this trade-off can be captured via a novel information-theoretical formulation for datasets with a known distribution. Moreover, for scenarios where the statistics of the dataset is unknown, we propose a new deep learning framework by leveraging a generative adversarial network approach, which allows the user to learn efficient schemes from the data itself. We evaluate the performance of the scheme on a synthetic Gaussian dataset as well as on the MNIST, CIFAR-10, and LSUN datasets. For the MNIST, CIFAR-10, and LSUN datasets, the data-driven approach significantly outperforms a nonlearning-based scheme which combines source coding with the download of multiple files.

Index Terms—Compression, data-driven framework, generative adversarial networks, generative adversarial privacy, information-theoretical privacy, private information retrieval.

I. INTRODUCTION

MACHINE learning (ML) has been recognized as a game-changer in modern information technology, and various ML techniques are increasingly being utilized for a variety of applications from intrusion detection to image classification. Efficient information retrieval (IR) from a single or several servers storing such datasets under a strict user privacy constraint has been extensively studied within the framework of private information retrieval (PIR). In PIR, first introduced by Chor *et al.* [1], a user can retrieve an arbitrary file from a dataset without disclosing any information (in an information-theoretical sense) about which file she is interested in to the servers storing the dataset. Typically, the size of the queries is much smaller than the size of a file. Hence, the efficiency of a PIR protocol is usually measured in terms of the download cost, or equivalently, the download (or PIR) rate, neglecting the upload cost of the queries. PIR

This work was supported in part by US NSF under Grant CNS-1813942. Also, the research presented in this article has benefited from the Experimental Infrastructure for Exploration of Exascale Computing (eX3), which is financially supported by the Research Council of Norway under contract 270053 (<https://www.ex3.simula.no/>). This paper was presented in part at the NeurIPS Workshop on Privacy Preserving Machine Learning - PRIML and PPML Joint Edition, Vancouver, BC, Canada, Dec. 11, 2020.

C.-W. Weng, Y. Yakimenka, H.-Y. Lin, and E. Rosnes are with Simula UiB, N-5006 Bergen, Norway (e-mail: chungwei@simula.no, yauhen@simula.no, lin@simula.no, eirikrosnes@simula.no).

J. Kliewer is with Helen and John C. Hartmann Department of Electrical and Computer Engineering, New Jersey Institute of Technology, Newark, New Jersey 07102, USA (e-mail: jkliewer@njit.edu).

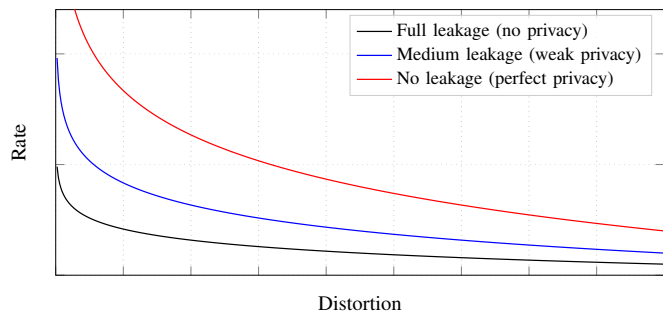


Fig. 1. The rate-distortion trade-off under different privacy levels.

has been studied extensively over the last decade, see, e.g., [2]–[7] and references therein.

Recently, there has been several works proposing to relax the perfect privacy condition of PIR in order to improve on the download cost, see, e.g., [8]–[13]. Inspired by this line of research, we propose to simultaneously relax both the perfect privacy condition and the perfect recovery condition, by allowing for some level of distortion in the recovery process of the requested file, in order to achieve even lower download costs (or, equivalently, lower download rates). This scenario is of interest in many real-world applications. For instance, a user may be willing to share the genre of a requested movie to the servers storing it (but not the exact identity of the movie) and may also wish to retrieve the movie under a small level of distortion as long as the retrieved quality is high enough, in order to reduce the required download time.

We concentrate on the practical scenario in which the dataset is stored on a single server, which is in alignment with the current research trend within the PIR literature as it is very difficult to ensure that the servers cannot collude in practice. For instance, typically all the servers are owned by one entity, e.g., Google, and then we cannot assume that they are independent.

Our main contributions are summarized as follows.

- A problem formulation with arbitrary distortion and leakage functions is presented, which establishes a trifold trade-off between download rate, privacy leakage to the server storing the dataset, and distortion in the recovery process for the user.
- We show that the optimal rate-distortion-leakage trade-off is convex and this allows us to further show a concise information-theoretical formulation in terms of mutual information (MI) in the limit of large file sizes (see Theorem 1). The typical behavior of a rate-distortion-leakage trade-off is illustrated in Fig. 1, showing that an increased

level of privacy leads to a higher rate-distortion trade-off curve, and hence a sacrifice in either download rate or distortion. Furthermore, a general achievable scheme combining source coding with the download of multiple files is proposed.

- To overcome the practical limitation of unknown statistical properties of real-world datasets, we consider a data-driven approach leveraging recent advancements in generative adversarial networks (GANs) [14], which allows a user to learn efficient schemes from the data itself. In our proposed novel GAN-based IR framework, learning can be phrased as a constrained minimax game between a user which desires to keep the identity of the requested file private and a server that tries to infer which file the user is interested in, under both a user distortion and a download rate constraint. Similar to [15], where a cross-entropy loss function is used as a discriminative classifier for unlabeled or partially labeled data, the server is modeled as a discriminator and trained with cross-entropy for labeled data. The data flow can be seen as similar to that of auxiliary classifier GANs [16], but with important differences in terms of, e.g., the loss function.
- We present numerical results for the MNIST [17], CIFAR-10 [18], and LSUN [19] datasets (the latter comprising 24 times as many images as CIFAR-10), showing that the data-driven approach significantly outperforms the proposed achievable scheme,¹ while for a synthetic Gaussian dataset, where the source statistics is known, it performs close to the proposed achievable scheme using a variant of the generalized Lloyd algorithm [20], [21] for the source code.

A. Related Work

As outlined above, in this work we consider “information retrieval” in the sense of PIR, while “information retrieval” in the traditional sense used by the *information retrieval community* has a different meaning. In particular, in the traditional sense “information retrieval” refers to the problem of providing a list of documents given a query and has a wide range of applications [22]. In [23], the authors proposed to iteratively optimize two well-established models of traditional IR; namely generative retrieval focusing on predicting relevant documents given a query and discriminative retrieval focusing on predicting document relevance given a query and document pair. The resulting optimization problem is formulated as a minimax game. Due to the differences in the system model there is no clear connection to our proposed framework, besides the formulation as a minimax game.

Preserving the privacy of sensitive information from publicly released datasets, while providing useful utility is a well-studied problem in the computer science literature. In contrast, the goal in this work is to preserve the privacy of requests. In [24], differential privacy [25], [26] is used as privacy metric and a fundamental trade-off between privacy and utility for statistical databases is presented. A similar privacy-utility

trade-off is also investigated in [27], but for another privacy measure and under an assumption that some prior knowledge about the data is known. Recently, this kind of problem is also studied for synthetic datasets in the ML literature [28], and it has been shown that it is related to rate-distortion theory and has a strong connection to the problem of robust ML [29]. Adversarial training is also applied for learning anonymized representations of a dataset, while protecting the private labels from an intermediate representation in [30]. In [31], adversarial training for preserving the privacy of visual recognition is adopted. An adversarial training framework that can simultaneously prevent leakage of private attributes and withstand reconstruction attacks was proposed in [32]. Lastly, we remark here that in our work, in contrast to the literature on adversarial training for privacy, the communication efficiency (in terms of download rate) of an IR scheme is considered an important performance metric.

Similar data-driven approaches, under the names of generative adversarial privacy [33], [34], privacy-preserving adversarial networks [35], and compressive privacy GAN [36], have recently been proposed for learning a privatization mechanism directly from the dataset in order to release it to the public and for generating compressed representations that retain utility while being able to withstand reconstruction attacks. A similar approach was also taken in [37] where a trifold trade-off between rate, distortion, and perception in lossy image compression was established.

Relaxing the perfect information-theoretical privacy condition by considering computationally-private IR, where the privacy relies on an intractability assumption (e.g., the hardness of deciding quadratic residuosity), has been investigated in several previous works, see, e.g., [38]–[40]. Hence, given infinite computational power, the requested file index can be determined precisely. Moreover, in [41], it was shown that allowing for side information can also decrease the download cost in single-server PIR. In [42], instead of keeping the identity of the requested file private, the authors propose to preserve the privacy of latent attributes of the user that are dependent on the retrieving requests. In contrast to these previous works, here we propose to relax the perfect reconstruction constraint in order to decrease the download cost. Moreover, to the best of our knowledge, extending PIR to *both* nonperfect privacy and recovery, specifically in a learning-based context by employing generative adversarial models, has not been addressed in the open literature so far.

II. PRELIMINARIES AND SYSTEM MODEL

A. Notation

We define $[a] \triangleq \{1, 2, \dots, a\}$. An arbitrary field is denoted by \mathbb{F} , while the set of nonnegative real numbers is denoted by $\mathbb{R}_{\geq 0}$. Vectors are denoted by bold letters and sets by calligraphic uppercase letters, e.g., \mathbf{x} and \mathcal{X} , respectively. We use uppercase letters for random variables (RVs) (either scalar or vector), e.g., X or \mathbf{X} . For a given index set \mathcal{I} , we write $X^{\mathcal{I}}$ to represent $\{X^{(m)} : m \in \mathcal{I}\}$. $\mathbf{E}_X[\cdot]$ and $\mathbf{E}_{P_X}[\cdot]$ denote expectation with respect to the RV X and the probability mass function (PMF) P_X , respectively. $\mathbf{H}(X)$ or $\mathbf{H}(P_X)$

¹The code for this work is available at https://github.com/Simula-UiB/GAUP_TIFS22.

represents the entropy of X , while $I(X;Y)$ denotes the MI between X and Y . The multivariate Gaussian distribution with mean $\boldsymbol{\mu}$ and covariance matrix Σ is denoted as $\mathcal{N}(\boldsymbol{\mu}, \Sigma)$. In particular, if the entries corresponding to this distribution are mutually independent, we have $\Sigma = \sigma^2 I$, for marginal standard deviation $\sigma \in \mathbb{R}_{\geq 0}$, where I denotes the identity matrix. The transpose of a vector is denoted as $(\cdot)^\top$, while the gradient of a function $f(x)$ is denoted by $\nabla f(x)$.

B. Single-Server Information Retrieval

Consider a dataset containing M files $\mathbf{X}^{(1)}, \dots, \mathbf{X}^{(M)}$ stored on a single server, where each file $\mathbf{X}^{(m)} = (X_1^{(m)}, \dots, X_\beta^{(m)})^\top$, $m \in [M]$, can be seen as a $\beta \times 1$ random vector (according to some probability distribution $P_{\mathbf{X}^{(m)}}$) over \mathbb{F}^β , where \mathbb{F} is any field (finite or infinite).² Assume that the user wishes to retrieve the M -th file, $M \in [M]$, where, for simplicity, M is assumed to be uniformly distributed over $[M]$.³ The formal definition of a general single-server IR scheme is as follows.

Definition 1. An IR scheme \mathcal{C} for a single server storing M files consists of: (i) a random strategy \mathcal{S} . (ii) A deterministic query function f_Q that generates a query $\mathbf{Q} = f_Q(M, \mathcal{S})$, for a requested file index M , where query \mathbf{Q} is sent to the server. (iii) A deterministic answer function f_A that returns the answer $\mathbf{A} = f_A(\mathbf{Q}, \mathbf{X}^{[M]})$ back to the user. (iv) A deterministic reconstruction function $\hat{\mathbf{X}} \triangleq f_{\hat{\mathbf{X}}}(\mathbf{A}, M, \mathbf{Q})$ giving an estimate of the desired file using the answer from the server together with the requested file index M and the query \mathbf{Q} .

Note that the server does not use \mathcal{S} directly to produce \mathbf{A} and thus using \mathbf{Q} is sufficient in the reconstruction.

We are interested in designing an IR scheme such that both the user's *utility* and *privacy* are preserved. On the one hand, this scheme should satisfy the condition of retrievability with a distortion measure $d(\cdot, \cdot)$, i.e.,

$$\mathbb{E}_{M, \mathbf{Q}, \mathbf{X}^{[M]}} [d(\mathbf{X}^{(M)}, \hat{\mathbf{X}})] \leq D, \quad (1)$$

where D is a given distortion constraint and $d(\mathbf{X}^{(M)}, \hat{\mathbf{X}}) = 1/\beta \sum_{i=1}^{\beta} d_i(X_i^{(M)}, \hat{X}_i)$, where $d_i : \mathbb{F} \times \mathbb{F} \rightarrow \mathbb{R}_{\geq 0}$ is a per-symbol distortion measure that is *translation invariant*, i.e., $d_i(x+z, \hat{x}+z) = d_i(x, \hat{x})$. For simplicity, we let $d_1 = \dots = d_\beta = d_{\text{sym}}$. On the other hand, the user would like to preserve her privacy with the query function, in the sense that the server should not be able to fully determine the identity M of the requested file. The server receives the query \mathbf{Q} , and the leakage is measured in terms of a leakage metric $\rho(P_{\mathbf{Q}|M})$. The query function should be designed such that

$$\rho(P_{\mathbf{Q}|M}) \leq L, \quad (2)$$

²With some abuse of wording, *dataset* refers to both the set of files $\mathbf{X}^{(1)}, \dots, \mathbf{X}^{(M)}$ and the training samples for the data-driven approach.

³Throughout the paper, we assume for simplicity that M is uniformly distributed and also that the file sizes are equal and fixed. The distribution P_M does not affect the generality of our results, and it is also common to have equal and fixed file sizes in the PIR literature. These assumptions can be lifted, which is referred to as semantic PIR in the literature [43].

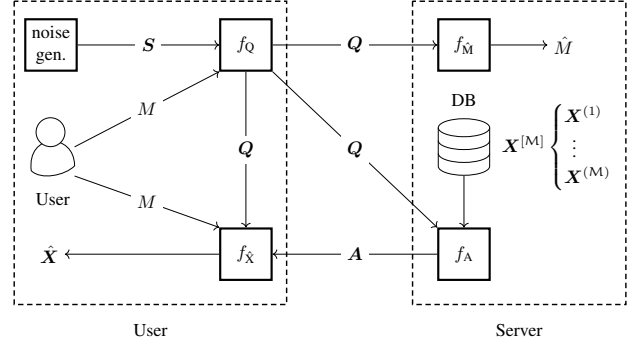


Fig. 2. IR scheme for an arbitrary dataset stored on a single server.

where L is the maximum allowed leakage.⁴

Moreover, it is worth mentioning that, unlike the setting of classical PIR, where perfect retrievability is ensured for every file, i.e., $\mathbb{E}_{\mathbf{Q}, \mathbf{X}^{[M]}} [d(\mathbf{X}^{(m)}, \hat{\mathbf{X}})] = 0$ for all $m \in [M]$, the distortions for different files need not to be equal. In other words, it is possible to have $\mathbb{E}_{\mathbf{Q}, \mathbf{X}^{[M]}} [d(\mathbf{X}^{(m)}, \hat{\mathbf{X}})] \neq \mathbb{E}_{\mathbf{Q}, \mathbf{X}^{[M]}} [d(\mathbf{X}^{(m')}, \hat{\mathbf{X}})]$ for $m \neq m'$, and (1) can be expressed as

$$\mathbb{E}_M \left[\mathbb{E}_{\mathbf{Q}, \mathbf{X}^{[M]}} [d(\mathbf{X}^{(M)}, \hat{\mathbf{X}}) \mid M = m] \right] \leq D.$$

Given a query function f_Q and an answer function f_A of an IR scheme, we measure its efficiency in terms of the download rate (in bits per symbol) defined as

$$\begin{aligned} \mathcal{R}(f_Q, f_A) &\triangleq \frac{\mathbb{E}_{\mathbf{Q}, \mathbf{A}} [\ell(\mathbf{A}) \mid \mathbf{Q}]}{\beta} = \frac{1}{\beta} \sum_{\mathbf{q}} P_{\mathbf{Q}}(\mathbf{q}) \mathbb{E}_{\mathbf{A}} [\ell(\mathbf{A}) \mid \mathbf{Q} = \mathbf{q}], \quad (3) \end{aligned}$$

where $\ell(\mathbf{A} = \mathbf{a}) \mid \mathbf{Q} = \mathbf{q}$ is the length of the answer \mathbf{a} for query \mathbf{q} .⁵

C. Problem Formulation

We consider a model that protects the privacy of the user against a honest-but-curious server. The IR model above guarantees that a user can retrieve an arbitrary file stored on a single server (with some distortion), while the server can only partially infer the identity of the requested file. In this work, we will study the trifold trade-off between download rate, expected distortion, and privacy leakage to the server for an IR scheme. In particular, for a given constraint D on the expected distortion $\mathbb{E}_{M, \mathbf{Q}, \mathbf{X}^{[M]}} [d(\mathbf{X}^{(M)}, f_{\hat{\mathbf{X}}}(\mathbf{A}, M, \mathbf{Q}))]$ for the retrieval of the requested file indexed by M and for a given constraint L on the leakage to the server $\rho(P_{\mathbf{Q}|M})$, the goal is to minimize the download rate $\mathcal{R}(f_Q, f_A)$. This can be formulated as the constrained optimization problem

$$\min_{(f_Q, f_A, f_{\hat{\mathbf{X}}})} \mathcal{R}(f_Q, f_A)$$

⁴Note that the leakage metric is a function of the probability distribution of $\mathbf{Q}|M$ and not the particular values. In other words, re-labeling queries in some bijective way does not change the leakage. For example, if instead of sending integers 1, 2, ..., the user starts sending strings "one", "two", ..., the leakage does not change.

⁵Note that we define the download rate in accordance with the rate-distortion literature, i.e., as the fraction between the expected download cost and the requested file size β , while in the PIR literature the download rate is defined as the inverse fraction, i.e., as the fraction between the requested file size and the expected download cost.

$$\begin{aligned}
\text{subject to } & \mathbb{E}_{M, \mathbf{Q}, \mathbf{X}^{[M]}} [d(\mathbf{X}^{(M)}, \hat{\mathbf{X}})] \leq D, \\
& \rho(P_{\mathbf{Q}|M}) \leq L, \hat{\mathbf{X}} = f_{\hat{\mathbf{X}}}(\mathbf{A}, M, \mathbf{Q}), \\
& \mathbf{Q} = f_{\mathbf{Q}}(M, \mathbf{S}), \mathbf{A} = f_{\mathbf{A}}(\mathbf{Q}, \mathbf{X}^{[M]}). \quad (4)
\end{aligned}$$

To further capture the information leakage for training, we define $\hat{M} \triangleq f_{\hat{M}}(\mathbf{Q})$ to be the server's inference of the user's requested file index M from the query \mathbf{Q} using a decision decoder $f_{\hat{M}}$. The proposed model is illustrated in Fig. 2.⁶ The leakage on the identity of the requested file can also be quantified by a loss function denoted as $f_{\text{Loss}}(M, \hat{M})$. Hence, the expected loss with respect to M and \mathbf{Q} is

$$\begin{aligned}
& J(f_{\mathbf{Q}}, f_{\hat{M}}) \\
& \triangleq \mathbb{E}_{M, \mathbf{Q}} [f_{\text{Loss}}(M, \hat{M})] = \mathbb{E}_{M, \mathbf{Q}} [f_{\text{Loss}}(M, f_{\hat{M}}(\mathbf{Q}))].
\end{aligned}$$

Here, the leakage metric $\rho(P_{\mathbf{Q}|M})$ in (2) is connected to the expected loss $J(f_{\mathbf{Q}}, f_{\hat{M}})$ as $\rho(P_{\mathbf{Q}|M}) = \max_{f_{\hat{M}}} J(f_{\mathbf{Q}}, f_{\hat{M}})$. Note that the main objective is to minimize the user's leakage to the server, which is equivalent to minimizing $\max_{f_{\hat{M}}} J(f_{\mathbf{Q}}, f_{\hat{M}})$, while the goal of the server is the opposite, i.e., of making the user's loss as large as possible or, equivalently, of maximizing $J(f_{\mathbf{Q}}, f_{\hat{M}})$.

D. Generative Adversarial Approach

The inference of the server can also be modeled in a generative adversarial fashion [33]–[36]. In particular, the *leakage-distortion* trade-off for any fixed download rate constraint R is formally described as follows. Consider a family of IR schemes with query generators $f_{\mathbf{Q}}$, answer functions $f_{\mathbf{A}}$, and with download rate $R(f_{\mathbf{Q}}, f_{\mathbf{A}})$ at most R . The goal of the server is to maximize the expected loss $J(f_{\mathbf{Q}}, f_{\hat{M}})$ of the user by designing the decision function $f_{\hat{M}}$. In contrast, the user would like to design a scheme with $f_{\mathbf{Q}}$, $f_{\mathbf{A}}$, and $f_{\hat{\mathbf{X}}}$ such that the download rate $R(f_{\mathbf{Q}}, f_{\mathbf{A}}) \leq R$ and such that the maximum expected loss $\max_{f_{\hat{M}}} J(f_{\mathbf{Q}}, f_{\hat{M}})$ is minimized, while preserving the utility of the scheme, i.e., the user can still retrieve the requested file with an expected distortion smaller than a prescribed D . This leads to the constrained minimax optimization problem

$$\min_{(f_{\mathbf{Q}}, f_{\mathbf{A}}, f_{\hat{\mathbf{X}}})} \max_{f_{\hat{M}}} J(f_{\mathbf{Q}}, f_{\hat{M}}) \quad (5a)$$

$$\begin{aligned}
\text{subject to } & \mathbb{E}_{M, \mathbf{Q}, \mathbf{X}^{[M]}} [d(\mathbf{X}^{(M)}, \hat{\mathbf{X}})] \leq D, \\
& R(f_{\mathbf{Q}}, f_{\mathbf{A}}) \leq R, \quad (5b)
\end{aligned}$$

$$\begin{aligned}
& \hat{\mathbf{X}} = f_{\hat{\mathbf{X}}}(\mathbf{A}, M, \mathbf{Q}), \mathbf{Q} = f_{\mathbf{Q}}(M, \mathbf{S}), \\
& \mathbf{A} = f_{\mathbf{A}}(\mathbf{Q}, \mathbf{X}^{[M]}). \quad (5c)
\end{aligned}$$

Note that the minimax formulation in (5a) can be written in a GAN form [14] in which $f_{\hat{M}}$ plays the role of the *discriminator* and $f_{\mathbf{Q}}$ plays the role of the *generator*. Thus, the machinery of

⁶In case the files are of different sizes, they can be dividing into different classes based on their sizes, and we would need a separate query function $f_{\mathbf{Q}}$ and decoding function $f_{\hat{\mathbf{X}}}$ for each class, while only a single answer function $f_{\mathbf{A}}$ and adversary function $f_{\hat{M}}$ would be required. Moreover, the distortion and leakage constraints in (1) and (2), respectively, and also the rate in (3) would be averages over the classes of files.

GANs can be used to determine the leakage-distortion trade-off. In doing so, (5) is first reformulated as the unconstrained optimization problem

$$\begin{aligned}
& \min_{(f_{\mathbf{Q}}, f_{\mathbf{A}}, f_{\hat{\mathbf{X}}})} \max_{f_{\hat{M}}} \left[J(f_{\mathbf{Q}}, f_{\hat{M}}) + \eta_1 \mathbb{E}_{M, \mathbf{Q}, \mathbf{X}^{[M]}} [d(\mathbf{X}^{(M)}, \hat{\mathbf{X}})] \right. \\
& \quad \left. + \eta_2 R(f_{\mathbf{Q}}, f_{\mathbf{A}}) \right], \quad (6)
\end{aligned}$$

where η_1 and η_2 are tuning parameters, and \mathbf{Q} and \mathbf{A} are according to Definition 1. The minimax game in (6) with soft decision decoding, i.e., with the log-loss function in (7), will be the basis for training, as described below in Section IV.

Note that the formulations in (5) and (4) are equivalent in the sense that they give raise to the same rate-distortion-leakage trade-off region. However, the second formulation in (5) is more amenable to learning as minimizing the rate as in (4) is difficult in a data-driven approach, while on the other hand, the first formulation in (4) is more amenable to theoretical analysis. The reason the formulation in (5) is more amenable to learning is that we can easily fix a rate constraint R by selecting the size of the output layer of the answer network and the number of quantizing levels $\kappa \geq 2$ used. See Section IV-A below for further details.

III. RATE-DISTORTION-LEAKAGE TRADE-OFF

In this section, we first show that the set of achievable rate-distortion-leakage triples (R, D, L) from (4) is a convex set. Then, we consider two different loss functions $f_{\text{Loss}}(m, \hat{M})$, the 0-1 loss and the log-loss. Next, we derive an expression for the optimal download rate $R(f_{\mathbf{Q}}, f_{\mathbf{A}})$ for datasets with M files where $\{X_i^{(1)}, \dots, X_i^{(M)}\}_{i=1}^{\beta} = \{X_i^{[M]}\}_{i=1}^{\beta}$ are independent and identically distributed (i.i.d.), and a known distribution. Finally, we present a general achievable scheme that can be applied to any dataset.

Lemma 1. *The set of achievable (feasible) rate-distortion-leakage triples (R, D, L) from (4) is a convex set, for any leakage metric ρ that is convex in $P_{\mathbf{Q}|M}$.*

Proof: See Appendix A. ■

We remark that the convexity definition of $\rho(\cdot)$ is according to the convexity property of MI [44, Ch. 2], i.e., the metric is called *convex* if $\rho(\lambda P_{\mathbf{Q}_i|M} + (1-\lambda)P_{\mathbf{Q}_0|M}) \leq \lambda \rho(P_{\mathbf{Q}_1|M}) + (1-\lambda)\rho(P_{\mathbf{Q}_0|M})$ for any $0 \leq \lambda \leq 1$, where $P_{\mathbf{Q}_i|M}$, $i \in \{0, 1\}$, are both defined over the same alphabet $[M] \times \mathcal{Q}$.

A. Loss Functions

Note that if $f_{\text{Loss}}(m, \hat{M})$ is the 0-1 loss function [45] it can be easily shown, following a similar argument as in [33, Sec. 2.2], that the optimal inference strategy for the server is the maximum a posteriori probability (MAP) decoder, and that the privacy metric $\rho(P_{\mathbf{Q}|M})$ in this case equals the server's *inference accuracy* $\Pr(M = \hat{M})$. This case is referred to as hard decision decoding.

In contrast to hard decision decoding where the server guesses exactly one file index from the query, we can also consider a soft decision decoding rule for the server. In this case, likelihoods for all file indices are computed by the

server, i.e., the server can infer a PMF $F_{\hat{M}}(\cdot|\mathbf{Q})$, where $\sum_m F_{\hat{M}}(m|\mathbf{Q}) = 1$. Let $f_{\text{Loss}}(m, \hat{M})$ be the log-loss function defined as

$$f_{\text{Loss}}(m, \hat{M}) = H(M) + \log F_{\hat{M}}(m|\mathbf{Q}), \quad (7)$$

i.e., the loss is zero when the server's guess is equally likely over $[M]$. Then, the expected loss function is equal to

$$\begin{aligned} J(f_Q, f_{\hat{M}}) &= H(M) - \sum_q \sum_m P_{M, \mathbf{Q}}(m, \mathbf{q}) \log \frac{1}{F_{\hat{M}}(m|\mathbf{q})} \\ &= H(M) - \sum_q P_Q(\mathbf{q}) \left(- \sum_m P_{M|\mathbf{Q}}(m|\mathbf{q}) \log F_{\hat{M}}(m|\mathbf{q}) \right) \\ &= H(M) - \sum_q P_Q(\mathbf{q}) H(P_{M|\mathbf{Q}=\mathbf{q}}(\cdot) \parallel F_{\hat{M}}(\cdot|\mathbf{q})) \end{aligned} \quad (8)$$

$$\begin{aligned} &\leq H(M) - \sum_q P_Q(\mathbf{q}) H(P_{M|\mathbf{Q}=\mathbf{q}}(\cdot)) \\ &= H(M) - \sum_q P_Q(\mathbf{q}) H(M | \mathbf{Q} = \mathbf{q}), \end{aligned} \quad (9)$$

where $H(P_X \parallel P_Y)$ denotes the cross-entropy between the distributions P_X and P_Y , and (9) follows since for any two distributions $P_X(\cdot)$ and $P_Y(\cdot)$, we have $H(P_X(\cdot) \parallel P_Y(\cdot)) \geq H(P_X(\cdot))$. Moreover, observe that

$$\max_{f_{\hat{M}}} (J(f_Q, f_{\hat{M}})) \leq H(M) - H(M | \mathbf{Q}) = I(M; \mathbf{Q}),$$

and from (9), it follows that equality holds if $P_{M|\mathbf{Q}=\mathbf{q}}(\cdot) = F_{\hat{M}}(\cdot|\mathbf{q})$. Therefore, under the log-loss function, the leakage to the server is measured in terms of MI, i.e., $\rho(P_{Q|M}) = I(M; \mathbf{Q})$, and the user wishes to minimize the MI leakage. This case is referred to as soft decision decoding. Moreover, this gives an explicit reason (see (8)) to use empirical categorical cross-entropy as loss function for the data-driven approach in Section IV.

Finally, note that it can be seen that Lemma 1 also holds for any loss function f_{Loss} , since any $\rho(P_{Q|M})$ that can be expressed via an expectation as $J(f_Q, f_{\hat{M}})$ is always convex in $P_{Q|M}$. Thus, in the rest of paper, we will always assume that the metric $\rho(\cdot)$ is convex in its argument.

B. Optimal Download Rate for Data With Known Distribution

Theorem 1. Assume that $\{X_i^{[M]}\}_{i=1}^\beta$ are i.i.d. and that for any $i \in [\beta]$, the RVs $\{X_i^{(m)}\}_{m=1}^M$ are distributed according to a prototype joint PMF $P_{X^{(1)}, \dots, X^{(M)}}$. Then, the download rate given in (4) equals

$$R(D, L) \triangleq \min_{P_{Q|M}, P_{\hat{X}^{[M]}|X^{[M]}, \mathbf{Q}} \in \mathcal{F}(D, L)} I(X^{[M]}; \hat{X}^{[M]} | \mathbf{Q}), \quad (10)$$

as $\beta \rightarrow \infty$, where

$$\mathcal{F}(D, L) \triangleq \left\{ P_{Q|M}, P_{\hat{X}^{[M]}|X^{[M]}, \mathbf{Q}} : \mathbb{E}_{M, \mathbf{Q}, X^{[M]}} [d_{\text{sym}}(X^{(M)}, \hat{X}^{(M)})] \leq D, \rho(P_{Q|M}) \leq L \right\}$$

is the set of feasible distributions $P_{Q|M}$ and $P_{\hat{X}^{[M]}|X^{[M]}, \mathbf{Q}}$ for which the joint distribution $P_{M, \mathbf{Q}, X^{[M]}, \hat{X}^{[M]}}$ satisfies the leakage and distortion constraints of $\mathcal{F}(D, L)$.

The proof that the rate R is bounded from below by $R(D, L)$, for any β , is given in Appendix B. We provide the following intuition based on information-theoretical considerations. Note that our single-server IR scheme can be seen as a source coding problem with side information, where the server and the user act as an encoder and a decoder, respectively, and where the query can be seen as a controllable side information known to both the encoder and decoder in order to enforce the privacy condition. This is similar to the well-known Wyner-Ziv problem [46]. Hence, a random-coding based scheme can be used to achieve $R(D, L)$ as $\beta \rightarrow \infty$. Further, it can be shown that the alphabet size of the designed queries can be restricted to $M + 3$, which follows from applying Carathéodory's theorem [44, Thm. 15.3.5]. Note, however, that finding a closed-form expression for $R(D, L)$ in our case is intractable. Hence, we provide numerical results for Gaussian data in Section V, which verify, by combining the achievable scheme proposed below in Section III-C with a convexifying approach, that (10) is indeed achievable.

C. Achievable Schemes

In this subsection, we present a general achievable scheme for an arbitrary number of files M and hard decision leakage (or accuracy) $L \in \{1, 1/2, 1/3, \dots, 1/M\}$.

The construction is based on the following fact. If $L = 1$, we have the problem of lossy compression: the user explicitly tells the server what she needs to download, and the server sends the requested data compressed with some pre-agreed method. One example of such compression is quantization. This scheme is designed against a maximum likelihood decoder that provides the best inference for the server. Assume that the user wishes to retrieve the M -th file and to ensure a leakage of $L = 1/N$, $1 \leq N \leq M$.

- The user first selects a lossy source coding scheme \mathcal{C} to encode (separately or together) N files of size β each. Assume that the source coding scheme achieves an average compression size (in bits) of $\log_2 |\mathcal{C}|$ and expected normalized distortion D (normalized by $N\beta$).
- The user's query is designed to exactly request N files with indices M_1, \dots, M_N such that $M \in \{M_1, \dots, M_N\}$, where the $N - 1$ nondesired indices are chosen uniformly at random. These $N - 1$ file indices are added in order to "trick" the server and hide the real file index M of interest.
- After receiving the queries sent by the user, the server compresses all N files by using the source coding scheme \mathcal{C} , and transmits the answer back to the user.
- The user decompresses the answer using the selected source coding scheme, and the $N - 1$ nondesired reconstructed files are discarded.

The rate of this IR scheme is $R = \log_2 |\mathcal{C}|/\beta$, and the expected distortion is D and the leakage is L . The performance of the scheme is strongly dependent on the used source coding scheme \mathcal{C} . If the distributions of the files differ significantly, a separate encoder for each subset $\{M_1, M_2, \dots, M_N\}$ will achieve better results compared to a single encoder for all N -subsets. Using Lemma 1, a scheme for any leakage $1/M \leq L \leq 1$ (not only reciprocal of an integer) can be constructed.

From the general scheme above, two specific schemes can be constructed based on the source coding scheme used. The first scheme is constructed by selecting a good source coding scheme for a finite β , e.g., a scheme based on quantization. In particular, for Gaussian data we use a variant of the generalized Lloyd algorithm [20], [21] in order to construct a good quantization scheme. In the sequel, we will refer to this scheme as the compression-based scheme (cf. Appendix C). The second scheme, referred to in the sequel as Shannon's scheme, assumes $\beta \rightarrow \infty$ and uses the well-known rate-distortion function from information theory for the source coding scheme [47]. In Fig. 3(a) below, combined with a convexifying approach described in Appendix C-B, we plot the performance of both schemes for a synthetic Gaussian dataset. It is worth mentioning that by numerically solving (10) for the considered Gaussian data, the lower bound and the approximation values of Shannon's scheme are actually quite close, which shows that Shannon's scheme performs very close to the information-theoretical optimum for the considered Gaussian data.

IV. DATA-DRIVEN APPROACH

In this section, we describe our new data-driven framework for constructing an efficient IR scheme for downloading an arbitrary file from an arbitrary dataset stored on a single server. The four functions in Fig. 2 are represented as deep neural networks and we assume, for now, that they have already been trained.

The user wishes to retrieve the M -th file $\mathbf{X}^{(M)}$ and encodes M as a one-hot $\mathbf{Y} = (Y_1, Y_2, \dots, Y_M) \in \{0, 1\}^M$, where $Y_j = 1$ if $j = M$, and $Y_j = 0$ otherwise. Next, the user generates a "noise" vector $\mathbf{S} = (S_1, S_2, \dots, S_M)$, where S_1, S_2, \dots, S_M are i.i.d. according to the standard Gaussian distribution $\mathcal{N}(0, 1)$. The concatenation $(S_1, S_2, \dots, S_M, Y_1, Y_2, \dots, Y_M)$ is the input to a deep neural network, representing the function f_Q , for query generation. This network produces the query \mathbf{Q} that is sent to the server. The intuition behind this neural network is to hide the value of M . The server's answer is produced by feeding the stored data $\mathbf{X}^{[M]}$ and the received query \mathbf{Q} into a deep neural network, representing the function f_A , for answer construction. The deep neural network produces the answer vector \mathbf{A} that is sent back to the user. The user then feeds \mathbf{A} and $(S_1, \dots, S_M, Y_1, \dots, Y_M)$ into a deep neural network for decoding, representing the function $f_{\hat{X}}$, to produce the estimate $\hat{\mathbf{X}}$ of the requested file $\mathbf{X}^{(M)}$.

On the server side, a deep neural network, representing the function $f_{\hat{M}}$, is used to guess the identity of the requested file. The input to the network is the query vector \mathbf{Q} and the output (using softmax) is a distribution-like vector $\mathbf{W} = \mathbf{W}(\mathbf{Q}) = (W_1, W_2, \dots, W_M)$, where $\sum_{j=1}^M W_j = 1$, $0 \leq W_j \leq 1$, and where W_j can be interpreted as "with probability/likelihood W_j , the user's requested file index M is equal to j ." The server's estimate of M is then $\hat{M} = \arg \max_{j \in [M]} W_j$.

A. Learning Algorithm

Training the deep neural networks representing the functions $f_Q, f_A, f_{\hat{X}}$, and $f_{\hat{M}}$ is done following (6) and (8) by first fixing

Algorithm 1 Training algorithm for generative adversarial user privacy

- 1: **Input:** Number of training samples n , training samples $\{(\mathbf{x}^{(1)}(l), \dots, \mathbf{x}^{(M)}(l))\}_{l \in [n]}$, number of training iterations T , size of minibatch for stochastic gradient descent b , and initial tuning parameter η_{initial}
 - 2: **Output:** $f_Q, f_A, f_{\hat{X}}$, and $f_{\hat{M}}$
 - 3: $t \leftarrow 1, \eta \leftarrow \eta_{\text{initial}}$
 - 4: Initialize the neural networks representing $f_Q, f_A, f_{\hat{X}}, f_{\hat{M}}$
 - 5: Initialize $\mathbf{q}_l^{(m)}$ and $\mathbf{a}_l^{(m)}$, $l \in [n]$, $m \in [M]$
 - 6: **while** $t \leq T$ **do**
 - 7: **for** $m \in [M]$ **do**
 - 8: Generate b noise samples $\{s_b\}_{b \in [b]}$ from $\mathcal{N}(\mathbf{0}, I)$
 - 9: **for** $b \in [b]$ **do**
 - 10: $\mathbf{q}_b^{(m)} \leftarrow f_Q(m, s_b)$
 - 11: **end for**
 - 12: **end for**
 - 13: Update $f_{\hat{M}}$ by stochastic gradient descent using
 - 14: $\nabla \left(\sum_{m \in [M]} \sum_{b \in [b]} \frac{1}{b \cdot M} \log w_m(\mathbf{q}_b^{(m)}) \right)$
 - 15: **for** $m \in [M]$ **do**
 - 16: Generate an index minibatch $\mathcal{B}^{(m)} \subseteq [n]$ of size b
 - 17: Generate b noise samples $\{s_b\}_{b \in \mathcal{B}^{(m)}}$ from $\mathcal{N}(\mathbf{0}, I)$
 - 18: **for** $b \in \mathcal{B}^{(m)}$ **do**
 - 19: $\mathbf{q}_b^{(m)} \leftarrow f_Q(m, s_b)$
 - 20: $\mathbf{a}_b^{(m)} \leftarrow f_A(\mathbf{q}_b^{(m)}, \mathbf{x}^{(1)}(b), \dots, \mathbf{x}^{(M)}(b))$
 - 21: **end for**
 - 22: **end for**
 - 23: Update $f_Q, f_A, f_{\hat{X}}$ by stochastic gradient descent using
 - 24: $\nabla \left(\sum_{m \in [M]} \sum_{b \in \mathcal{B}^{(m)}} \frac{1}{b \cdot M} \left[\log w_m(\mathbf{q}_b^{(m)}) + \eta \cdot d(\mathbf{x}^{(m)}(b), f_{\hat{X}}(\mathbf{a}_b^{(m)}, m, \mathbf{q}_b^{(m)})) \right] \right)$
 - 25: Update the tuning parameter η
 - 26: $t \leftarrow t + 1$
 - 27: **end while**
 - 28: **Return:** $f_Q, f_A, f_{\hat{X}}$, and $f_{\hat{M}}$
-

a download rate constraint R and then solving the minimax optimization problem

$$\min_{(f_Q, f_A, f_{\hat{X}})} \max_{f_{\hat{M}}} \frac{1}{n \cdot M} \sum_{m=1}^M \sum_{l=1}^n \left[-f_{\text{XE-Loss}}(\mathbf{y}^{(m)}(l), \mathbf{w}) + \eta \cdot d(\mathbf{x}^{(m)}(l), \hat{\mathbf{x}}) \right], \quad (11)$$

where $f_{\text{XE-Loss}}(\mathbf{y}^{(m)}(l), \mathbf{w}) = -\sum_{j=1}^M y_j^{(m)}(l) \log w_j = -\log w_m$ measures the categorical cross-entropy between $\mathbf{y}^{(m)}(l) = (y_1^{(m)}(l), \dots, y_M^{(m)}(l))$ and the corresponding $\mathbf{w} = (w_1, \dots, w_M)$ at the output of the adversary network, and n is the number of training samples. Here, $(\mathbf{x}^{(1)}(l), \dots, \mathbf{x}^{(M)}(l))$ denotes the l -th training sample, $l \in [n]$, and $\mathbf{y}^{(m)}(l)$ is the corresponding \mathbf{y} -vector when requesting the m -th file. The parameter η is a trade-off coefficient that is slightly increased in every epoch (typically by a value in the range from 0.00005 to 0.0005, depending on the actual learning scenario). The initial value of η is typically picked in the range from 0.1 to 2. The rate is computed based on the dimension of the answer network's output and the corresponding quantizer

levels like [37], [48]. In particular, the quantization in the forward direction (but after the sigmoid activation of the output layer) is done by nearest-neighbor assignment with a uniformly distributed noise added in order to improve the training, i.e., the i -th quantized output during training is $a_i^f = \arg \min_{\ell \in \mathcal{L}} \|\tilde{a}_i - \ell\|_2 + \text{Uniform}([-1/2(\kappa-1), 1/2(\kappa-1)])$, where $\mathcal{L} = \{\ell_1, \dots, \ell_\kappa\}$ is a *fixed* set of $\kappa \geq 2$ linearly equally spaced quantization points in the output range $[0, 1]$ of the sigmoid function (i.e., $\ell_i = (i-1)/(\kappa-1)$ for $i \in [\kappa]$), \tilde{a}_i denotes the i -th output of the sigmoid activated output layer, $\text{Uniform}(\mathcal{X})$ denotes a RV that is uniformly distributed over the set \mathcal{X} , and $\|\cdot\|_p$ is the ℓ^p -norm. Here, the width of the added uniformly distributed noise is set to be the same as the distance between two quantization points ($1/(\kappa-1)$) [49]. In the testing phase, no noise is added to the quantized output. In order to compute gradients in the backward pass, we use the differential “soft” assignment

$$a_i^b = \sum_{j=1}^{\kappa} \frac{e^{-\|\tilde{a}_i - \ell_j\|_1}}{\sum_{l=1}^{\kappa} e^{-\|\tilde{a}_i - \ell_l\|_1}} \ell_j \approx a_i^f$$

as an approximation to the nearest-neighbor assignment with noise, or a_i^f . The quantization scheme described above follows [37, App. E] (see also [48]).

To fix the rate, we fix the dimension of the answer network’s output layer and also the corresponding number of quantizing levels κ , which gives an upper bound on the operational rate in (3), and the rate constraint of (5b) can be easily enforced. To vary the fixed rate, we vary the dimension of the answer network’s output layer with $\kappa = 2$. The solution to the mini-max optimization problem in (11) is found using an iterative algorithm employing minibatch stochastic gradient descent outlined in Algorithm 1, which is similar to [33, Alg. 1]. In particular, the solution is found by first maximizing the objective function of (11) to determine the optimal f_M for a fixed initial triple (f_Q, f_A, f_X) . Next, the optimal triple (f_Q, f_A, f_X) is found for the given f_M from the previous step by minimizing the same objective function. This iterative process is continued until convergence or the maximum number of iterations is exceeded. Note that, although training is done based on a log-loss function (see (7)), we evaluate the performance more intuitively using accuracy, i.e., $\Pr(M = \hat{M})$, in Section V below.

V. NUMERICAL RESULTS

We demonstrate the application of our proposed data-driven approach to a synthetic Gaussian dataset and also to the MNIST, CIFAR-10, and LSUN datasets, showing that guaranteeing a certain privacy level leads to a higher rate-distortion trade-off curve, and hence a sacrifice in either download rate or distortion. We refer the reader to Appendix D for further details of the learning. The LSUN dataset is considered a large-scale dataset (comprising 24 times as many images as CIFAR-10), and in order to expedite the learning, we consider a downsized version comprising 64×64 pixels color images. We also remark here that training with very large file sizes is not the main target application area for this framework. However, in case we do have very large files, the files can be

split into smaller blocks and then we can train a scheme for the smaller blocks as outlined in [50, Sec. VI-A], e.g., a 128×128 pixels image can be split into 4 separate smaller 64×64 pixels sub-images. The resulting overall scheme has the same rate, distortion, and leakage as the small scheme trained on blocks considered as independent images. We also compare the data-driven approach with both the compression-based scheme (for all datasets) and Shannon’s scheme (for the Gaussian dataset) of Section III-C. The Gaussian dataset consists of $M = 4$ files, each of dimension $\beta = 3$ and drawn independently according to $\mathcal{N}(\boldsymbol{\mu}^{(m)}, \sigma^2 I)$, where $\boldsymbol{\mu}^{(1)} = (3, 3, 3)^\top$, $\boldsymbol{\mu}^{(2)} = (3, -3, -3)^\top$, $\boldsymbol{\mu}^{(3)} = (-3, 3, -3)^\top$, $\boldsymbol{\mu}^{(4)} = (-3, -3, 3)^\top$, and $\sigma = 3$. We pre-generated 1000000 (100000) data points for training (testing), 250000 (25000) for each of the $M = 4$ files. For MNIST, CIFAR-10, and LSUN, $M = 10$ (corresponding to the number of digits/classes), the training set is comprised of respectively $n = 6000, 5000, \text{ and } 120000$ images of size $28 \times 28, 32 \times 32, \text{ and } 64 \times 64$ pixels for each digit/class, and testing is performed on randomly chosen images from 1000 test images from each digit/class for MNIST and CIFAR-10 and from 4000 test images from each class for LSUN. The distortion between a requested file $\mathbf{X}^{(m)}$ and its estimate $\hat{\mathbf{X}}$ is measured as the per-symbol squared error.

In Fig. 3, we plot the accuracy, or $\Pr(M = \hat{M})$, as function of per-symbol squared error distortion for different download rates R for the data-driven approach (solid curves) and the compression-based scheme (dashed and dash-dotted curves). For MNIST a symbol is a gray-scale pixel, for CIFAR-10 and LSUN a pixel of each color, while for the Gaussian dataset it is a one-dimensional Gaussian RV. As a comparison, for the Gaussian dataset, we also plot the performance of Shannon’s scheme (dotted curves), assuming $\beta \rightarrow \infty$, as outlined in Section III-C. For Shannon’s scheme, we use the *information rate*, denoted by R_{inf} and defined as $H(\mathbf{A}|\mathbf{Q})/\beta$. It is well-known that the information rate is a true lower bound on the *operational* rate from (3) (cf. [44]).

As expected, one can have a higher privacy level (i.e., smaller leakage) for a given distortion at the expense of a higher download rate. For the MNIST dataset, for both $R = 1/2$ and $R = 1/8$, the data-driven approach significantly outperforms the compression-based scheme, while for the Gaussian dataset it performs close to the compression-based scheme using a variant of the generalized Lloyd algorithm [20], [21] for the source code. This should not come as a surprise, as for the Gaussian dataset, the probabilistic model is simple and known precisely. In particular, we believe that the generalized Lloyd algorithm provides close-to-optimal compression (cf. [51]). Note that as the exact operational rate for the data-driven curves could potentially be lower, the actual gap to Shannon’s scheme could in fact be smaller. For MNIST we combined JPEG-like compression (including discrete-cosine transform), run-length encoding, and other entropy coding techniques for the compression-based scheme (cf. [52, Sec. 8.2]). However, due to a very small size of images, the constant overhead (e.g., for storing the Huffman codebook) turned out to be unacceptably high. It is a well-known phenomenon that sophisticated compression methods work well only on files of medium and large size. We thus opted for scalar quantization

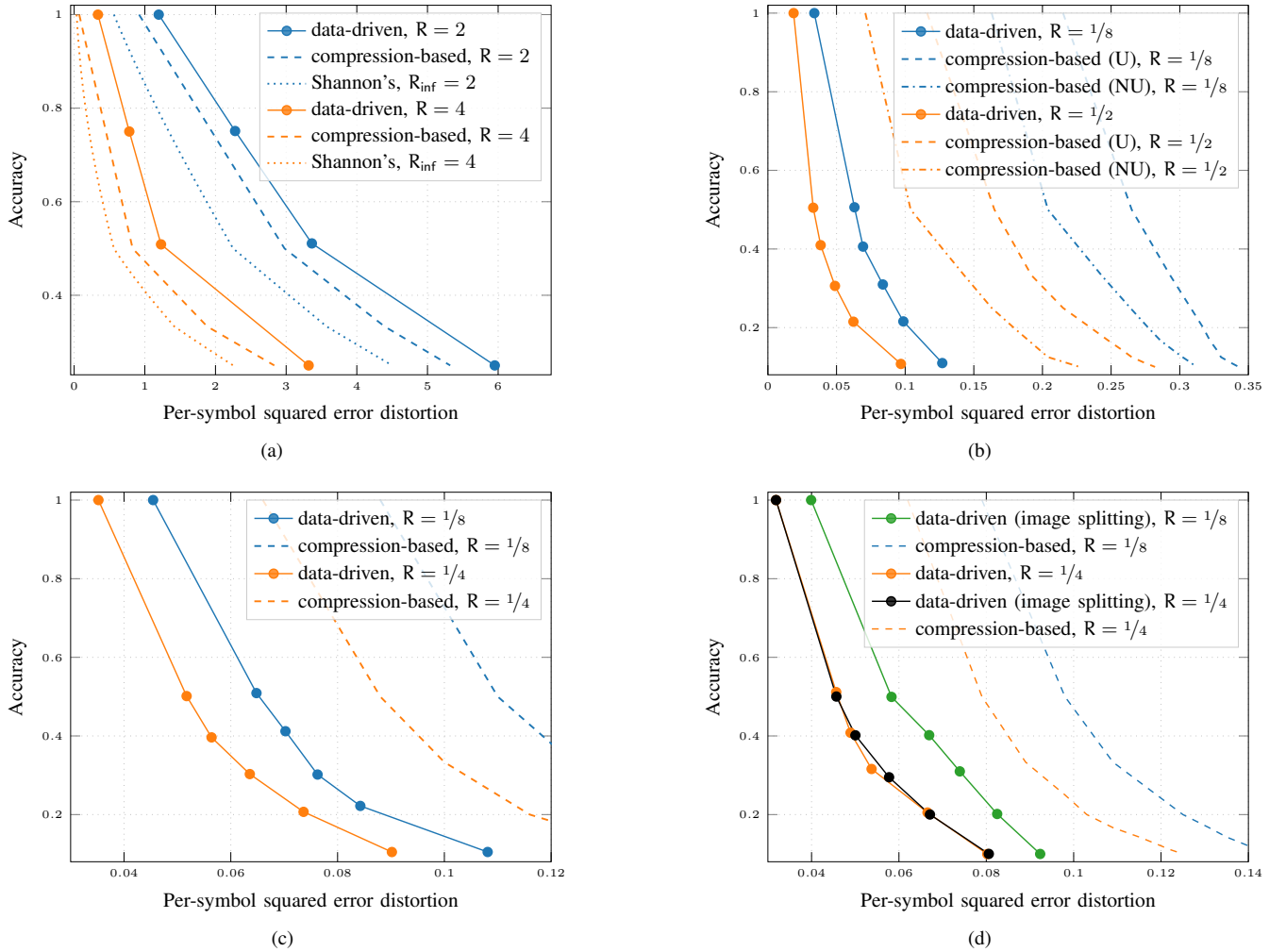


Fig. 3. Accuracy versus per-symbol squared error distortion for both the data-driven approach and the schemes from Section III-C. (a) Synthetic Gaussian dataset. (b) MNIST (U and NU stand for uniform and nonuniform quantization, respectively, cf. Appendix C-C). (c) CIFAR-10. (d) LSUN.

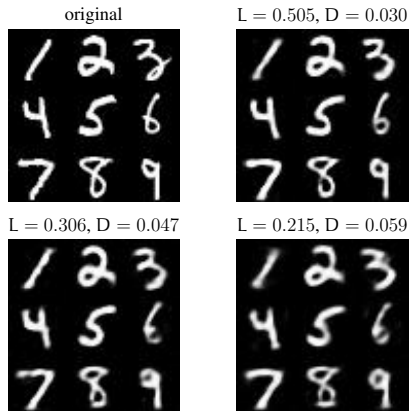
(see Appendix C-C for details). Fig. 4 depicts an example of the reconstructed digits for three levels of distortion D (with respect to the original digits displayed in the figure) and accuracy L for a download rate of $R = 1/2$ for the MNIST dataset. These reconstructions were obtained by the data-driven approach.

For CIFAR-10, we have considered the two download rates $R = 1/4$ and $R = 1/8$. The compression-based scheme for CIFAR-10 is rather similar to the scheme for MNIST (see Appendix C-D). The data-driven approach, again, outperforms the compression-based scheme for both rates considered with a gap similar to the one for MNIST.

As for CIFAR-10, we have considered $R = 1/4$ and $R = 1/8$ for LSUN. Moreover, we have considered the same compression-based scheme as for CIFAR-10 (see Appendix C-D). For $R = 1/4$, as can be seen from Fig. 3(d), the data-driven approach outperforms the compression-based scheme for all considered distortion constraints, with a performance gain that is comparable to that of the two previous image datasets. For comparisons, we have also shown the performance of the data-driven approach with image splitting

mentioned above, where the images are split into 4 separate smaller 32×32 pixels sub-images. The resulting 32×32 pixels sub-images, treated as independent images, are used to train the same neural network architecture (see Table V in Appendix D for further details) as for CIFAR-10. As can be seen from the figure, the splitting approach performs almost as well as training on the original images. This shows that image splitting is a powerful approach when having larger image sizes and also that the neural network architecture is robust across different classes of fixed-size images. For $R = 1/8$, the data-driven approach with image splitting outperforms the compression-based scheme, as for $R = 1/4$. We also note that the approach of splitting a 64×64 pixels image into 4 separate 32×32 pixels sub-images does not change much for the compression-based scheme, as the scheme splits the images into blocks anyway. The only potential difference would be for extremely low rates (e.g., 1 bit per whole image) when blocks of sizes larger than 32×32 pixels are required.

So far only the download cost of the proposed schemes has been considered, neglecting both the query upload cost and the cost of distributing the trained neural networks. First, the cost

Fig. 4. MNIST, $R = 1/2$ bits per pixel.

of distributing the trained networks can be neglected since training is usually done beforehand on a dedicated training server and can hence be seen as a one-time cost. This cost vanishes as the protocol can in principle run for a very long time serving a large number of users while the dataset grows continuously. Second, the query upload cost, i.e., $H(\mathbf{Q})$ (in bits), is in most cases much smaller than the download cost of the answers. As we will show below, this is also the case here for MNIST, CIFAR-10, and LSUN. For completeness, the one-time cost (in bits) of distributing the query and decoder networks to the user is 465479×32 , 1259135×32 , 744882×32 , and 9532703×32 bits for the Gaussian ($R = 2$), MNIST ($R = 1/2$), CIFAR-10 ($R = 1/8$), and LSUN ($R = 1/4$) datasets, respectively, while the corresponding one-time cost of distributing the answer generation network to the server is 532230×32 ($R = 2$), 7336888×32 ($R = 1/2$), 55871908×32 ($R = 1/8$), and 47357034×32 ($R = 1/4$) bits, respectively. These numbers are the sizes of the corresponding neural networks as reported by TensorFlow times 32 (the neural networks' edge weights are represented as 32-bits floats).

The number of neurons of the output layer of the query network is at most equal to the number of files M . Hence, the upload cost is at most $32 \cdot M$ (assuming 32-bits floats). For MNIST, this yields at most $32 \cdot 10 = 320$ bits, while the download cost is $28 \cdot 28 \cdot 1/2 = 392$ bits (assuming $R = 1/2$), which is higher. Downloading the entire dataset requires an overall communication cost of $28 \cdot 28 \cdot 8 \cdot 10 = 62720$ bits uncompressed, which is significantly higher. This number can be further reduced using lossless compression. The average losslessly compressed (with the LZMA algorithm [53, Sec. 3.24]) sizes for different digits range from 1358 (digit 1) to 2151 (digit 8), which sum up to 19007 bits for all 10 digits. In other words, a one instance of the dataset (10 files) can be downloaded as 19007 bits (on average), which is again significantly higher than the download cost. Analogously, one instance of the CIFAR-10 dataset (10 files) has the size of $32 \cdot 32 \cdot 3 \cdot 8 \cdot 10 = 245760$ bits, but can be on average compressed into 197207 bits, while one instance of the LSUN dataset, with an original size of $64 \cdot 64 \cdot 3 \cdot 8 \cdot 10 = 983040$ bits, has a mean compressed size of 721726 bits. In general, the upload cost scales linearly with the number of files and is independent of the file size, while the download cost increases

TABLE I
ESTIMATED MAP ADVERSARY ACCURACY FOR THE GAUSSIAN DATASET
WITH DIFFERENT VALUES OF (R, D, L) .

Gaussian dataset and $R = 2$			
D	5.95	3.36	2.28
L_{MAP}	0.25	0.53	0.75
L	0.25	0.51	0.75
Gaussian dataset and $R = 4$			
D	3.32	1.23	0.78
L_{MAP}	0.25	0.51	0.75
L	0.25	0.51	0.75

with the file size. In most cases, the file size is much larger than the number of files which is the standard argument for not considering the upload cost. In the embedded table below we summarize the different costs (in bits) for the Gaussian, MNIST, CIFAR-10, and LSUN datasets and compare with the cost (in bits) of downloading the entire dataset using lossless source coding. The upload cost is at most equal to the number of neurons of the query network's output layer times 32, with equality for a uniform query distribution.

	Download cost	Upload cost	Download dataset
Gaussian	6 (2), 12 (4)	≤ 128	384
MNIST	98 ($1/8$), 392 ($1/2$)	≤ 160	19007
CIFAR-10	384 ($1/8$), 768 ($1/4$)	≤ 160	197207
LSUN	1536 ($1/8$), 3072 ($1/4$)	≤ 160	721726

A. ML-Based Framework for Privacy Leakage

Since the derivative of $\Pr(M = \hat{M})$ is not well-defined, using an ML-based training approach to provide information-theoretical privacy guarantees has been substantially discussed in [33], [35], [36]. In this subsection, in order to assess the quality of training using an MI-based loss function, we tabulate in Tables I and II the estimates of the inference accuracy of a MAP adversary for M , denoted by L_{MAP} , operating directly on the queries from the query network for different datasets and for different levels of per-symbol squared error distortion D . The results for the Gaussian dataset are tabulated in Table I, while those for the MNIST, CIFAR-10, and LSUN datasets can be found in Table II.⁷ The estimates have been found by Monte-Carlo simulation of the networks, i.e., by repeatedly generating queries and estimating the probability density functions of the RVs $\mathbf{Q} | M$. The distortion values are averaged over the datasets as opposed to the distortion values reported in Fig. 4. For comparison we also show the inference accuracy L of the adversary network in Tables I and II. As can be seen by comparing the second and third lines of the tables, the inference accuracy of the adversary network is close to the inference accuracy of a MAP adversary. These results indicate that the ML-based model $f_{\hat{M}}$ is trained quite well and that the proposed ML-based framework is able to provide meaningful privacy guarantees.

⁷In the special case of full leakage, the problem reduces to the classical rate-distortion problem, and to improve performance, we only considered an encoder (for compression of the requested file), corresponding to f_A , and a decoder (for decompression at the user side), corresponding to $f_{\hat{X}}$. Hence, $L = L_{\text{MAP}} = 1$ in this special case.

TABLE II
ESTIMATED MAP ADVERSARY ACCURACY FOR THE MNIST, CIFAR-10,
AND LSUN DATASETS WITH DIFFERENT VALUES OF (R, D, L).

MNIST dataset and R = 1/2					
D	0.097	0.062	0.049	0.038	0.033
L _{MAP}	0.113	0.220	0.315	0.413	0.509
L	0.108	0.215	0.306	0.410	0.505
MNIST dataset and R = 1/8					
D	0.127	0.099	0.084	0.070	0.063
L _{MAP}	0.131	0.223	0.320	0.417	0.515
L	0.110	0.216	0.310	0.406	0.506
CIFAR-10 dataset and R = 1/4					
D	0.090	0.074	0.064	0.056	0.052
L _{MAP}	0.116	0.207	0.318	0.411	0.513
L	0.105	0.207	0.303	0.396	0.501
CIFAR-10 dataset and R = 1/8					
D	0.108	0.084	0.076	0.070	0.065
L _{MAP}	0.118	0.232	0.313	0.427	0.515
L	0.105	0.222	0.302	0.412	0.509
LSUN dataset with R = 1/4					
D	0.080	0.067	0.054	0.049	0.046
L _{MAP}	0.100	0.226	0.325	0.419	0.527
L	0.100	0.205	0.316	0.408	0.512
LSUN dataset with R = 1/4, image splitting					
D	0.081	0.067	0.058	0.050	0.046
L _{MAP}	0.100	0.220	0.317	0.415	0.521
L	0.100	0.200	0.295	0.402	0.500
LSUN dataset with R = 1/8, image splitting					
D	0.092	0.083	0.074	0.067	0.058
L _{MAP}	0.100	0.216	0.329	0.416	0.521
L	0.100	0.202	0.310	0.402	0.499

B. Heat Map Representation of the Answer

In order to gain insight about the learned data-driven schemes, we consider CIFAR-10 and analyze the output of the *first* network of the answer generation function (see Appendix D) through a heat map. The heat map reflects the contribution of each stored image in the answer, for a given requested image (corresponding to a given row of the heat map). Denote by $\delta^{(1)}, \dots, \delta^{(M)}$ the outputs from the M neurons following the softmax activation functions of the first network of the answer generation function. The second network of the answer generation function extracts the features of the dataset, denoted by $\mathbf{Z}^{(1)}, \dots, \mathbf{Z}^{(M)}$, which are fed as input to the third network of the answer generation function together with $\delta^{(1)}, \dots, \delta^{(M)}$ and the queries (which are fed into the fourth layer). In the second layer (of the third network), the vector $(\delta^{(1)}, \dots, \delta^{(M)})$ is multiplied elementwise with the feature vector $(\mathbf{Z}^{(1)}, \dots, \mathbf{Z}^{(M)})$, producing the vector $(\delta^{(1)}\mathbf{Z}^{(1)}, \dots, \delta^{(M)}\mathbf{Z}^{(M)})$, which is subsequently combined with the queries in the fifth layer in order to produce the final answer. Now, if $\delta^{(m)}$, for some $m \in [M]$, is close to zero, then the answer will not depend much on the file indexed by m , and it follows that the heat map indeed reflects which files contribute the most to the generated answer.

The heat map is shown in Fig. 5 for $(L, D, R) = (0.303, 0.064, 1/4)$, where each row corresponds to a requested image. The answer retrieve index (the label of the x -axis)

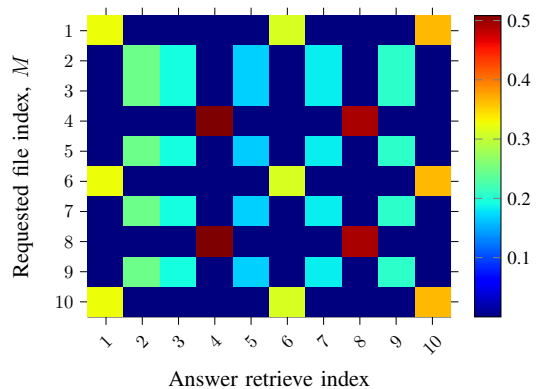


Fig. 5. Heat map with CIFAR-10 for leakage $L = 0.303$, distortion $D = 0.064$, and rate $R = 1/4$.

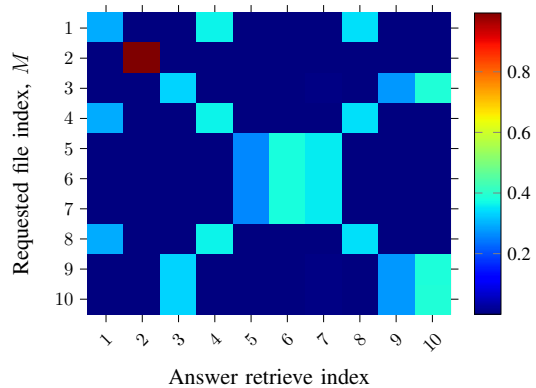


Fig. 6. Heat map with CIFAR-10 for leakage $L = 0.396$, distortion $D = 0.056$, and rate $R = 1/4$.

refers to the index of the softmax output values from the first network of the answer function, while the color reflects the actual softmax value in the sense that a warmer color indicates a higher value. As an example, consider rows 1, 6, and 10 (corresponding to $M = 1, 6,$ and 10). According to the heat map, the corresponding answers are functions of the files $\mathbf{X}^{(1)}, \mathbf{X}^{(6)},$ and $\mathbf{X}^{(10)}$, meaning that the server can infer that the user is requesting one of these files, but not exactly which one, giving an accuracy of $1/3$. By looking at the remaining rows, the overall (average) accuracy becomes $L = 3/10 \cdot 1/3 + 5/10 \cdot 1/5 + 2/10 \cdot 1/2 = 3/10$. Note that the scheme in this case is similar to the compression-based scheme from Section III-C and resembles time-sharing of three different schemes with $L = 1/3, 1/5,$ and $1/2$, respectively. Also, averaging the expected distortion values of the schemes for a given requested index gives exactly $D = 0.064$ (see Lemma 1).

In Fig. 6, the heat map with CIFAR-10 for $(L, D, R) = (0.396, 0.056, 1/4)$ is shown. As an example, consider rows 1, 4, and 8 (corresponding to $M = 1, 4,$ and 8). According to the heat map, the corresponding answers are functions of the files $\mathbf{X}^{(1)}, \mathbf{X}^{(4)},$ and $\mathbf{X}^{(8)}$, meaning that the server can infer that the user is requesting one of these files, but not exactly which one, giving an accuracy of $1/3$. For $M = 2$ (corresponding to the second row), however, the answer depends only on the second file, meaning that the server can infer that the user is requesting the second file, giving an accuracy of 1. By looking at the remaining rows, the overall (average) accuracy becomes $L = 3/10 \cdot 1/3 + 3/10 \cdot 1/3 + 3/10 \cdot 1/3 + 1/10 \cdot 1 = 4/10$.

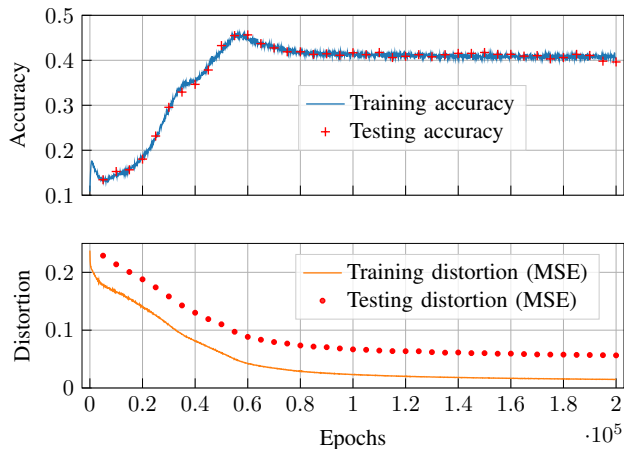


Fig. 7. Learning curves with CIFAR-10 for leakage $L = 0.396$, distortion $D = 0.056$, and rate $R = 1/4$.

C. Discussion on the Generative Adversarial Training

To investigate the well-known overfitting problem in ML [54], we show some learning curves with the CIFAR-10 dataset (for leakage $L = 0.396$, distortion $D = 0.056$, and rate $R = 1/4$) in Fig. 7. The training distortion and training adversary accuracy curves are averaged over a sliding window of length 100 and then sampled every 100 epoch. The testing distortion and testing adversary accuracy curves are sampled every 5000 epoch. Note that the distortion is measured in terms of mean squared error (MSE). If overfitting happened, then the testing distortion would increase while the training distortion would decrease with the number of epochs. This does not happen in our case. In fact, the testing distortion curve is decreasing and close to the training distortion curve. Hence, the level of overfitting is negligible. Moreover, training and testing accuracy values are close.

The mode collapse issue in GANs is well-known [55], [56]. Mode collapse means that the generator finds some weak point of the discriminator and keeps producing this mode of output to trick the discriminator. This may happen when the generator tries to fool the discriminator trained on a real dataset and causes problems because a GAN model is typically required to have diversity in its output. Techniques such as minibatch discrimination [55] can be applied to prevent mode collapse. However, note that in our setup mode collapse is less relevant (and may even be beneficial in some cases) as we in general do not need to have diversity in the query generation. In fact, a scheme for the MNIST (or CIFAR-10 or LSUN) dataset producing a deterministic query is a valid scheme with MAP adversary accuracy $L_{\text{MAP}} = 1/10$, while a scheme giving a one-to-one correspondence between M and $Q | M$ is also valid and gives MAP adversary accuracy $L_{\text{MAP}} = 1$. In order to investigate mode collapse in more detail for intermediate values of the accuracy, we have estimated the variance $\text{Var}[Q | M]$ for CIFAR-10 for leakage $L = 0.396$, distortion $D = 0.056$, and rate $R = 1/4$. The estimated values are from 10^6 samples and are tabulated in Table III. Here, $Q | M$ is a 5-dimensional vector since there are 5 neurons in the output layer of the query generator network in Table V. As can be seen from the table, the query network

TABLE III
QUERY VARIANCES FOR A GIVEN REQUESTED FILE INDEX FOR CIFAR-10 WITH $(L, D, R) = (0.396, 0.056, 1/4)$.

$M = m$	$\text{Var}[Q M = m]$
1	(0.000, 0.000, 0.081, 0.036, 0.001)
2	(0.049, 0.007, 0.024, 0.108, 0.000)
3	(0.041, 0.040, 0.090, 0.004, 0.079)
4	(0.000, 0.000, 0.081, 0.035, 0.001)
5	(0.027, 0.041, 0.000, 0.023, 0.001)
6	(0.027, 0.041, 0.000, 0.023, 0.001)
7	(0.027, 0.041, 0.000, 0.023, 0.001)
8	(0.000, 0.000, 0.080, 0.035, 0.001)
9	(0.041, 0.040, 0.091, 0.005, 0.081)
10	(0.040, 0.039, 0.091, 0.005, 0.081)

generates queries with some diversity. Moreover, from the MAP accuracy values L_{MAP} in Table II (for CIFAR-10 with $(L, D, R) = (0.396, 0.056, 1/4)$ it is 0.411), it follows that the discriminator is trained quite well and do not appear to suffer from degeneration in the query generation training due to mode collapse.

VI. CONCLUSION

In this work, we have studied the trade-off between download rate, privacy leakage to the server, and reconstruction distortion at the user for single-server IR schemes. An IR scheme can be seen as an extension of the well-known concept of PIR by allowing for distortion in the retrieval process and relaxing the perfect privacy requirement. An information-theoretical formulation for the trade-off in terms of MI has been provided in the limit of a large file size. We have shown that generative adversarial models can be successfully applied to design efficient single-server IR schemes. This is in particular beneficial if the data statistics is unknown. The main ingredient is a new optimization approach which combines GANs with additional constraints for the download rate and the desired reconstruction distortion at the user. We have shown that our proposed GAN-based data-driven approach for a fixed download rate is able to provide a trade-off between distortion for the user and privacy leakage to the server that is close to that of a proposed compression-based scheme for Gaussian data where the source statistics is known. A similar trade-off as for the Gaussian case can be observed if the proposed data-driven approach is applied to real-world datasets like MNIST, CIFAR-10, and LSUN, for which it significantly outperforms the compression-based scheme.

APPENDIX A PROOF OF LEMMA 1

Assume the schemes that achieve the triples (R_0, D_0, L_0) and (R_1, D_1, L_1) are \mathcal{C}_0 and \mathcal{C}_1 , respectively. We denote the queries of \mathcal{C}_0 and \mathcal{C}_1 as Q_0 and Q_1 , respectively. From \mathcal{C}_0 and \mathcal{C}_1 , we construct a new scheme \mathcal{C}_λ that achieves the triple $(\lambda R_1 + (1 - \lambda)R_0, \lambda D_1 + (1 - \lambda)D_0, \lambda L_1 + (1 - \lambda)L_0)$, for any $0 \leq \lambda \leq 1$. This is exactly the definition of a convex set. The scheme \mathcal{C}_λ is as follows.

- The user generates a time-sharing RV K according to the distribution

$$P_K(k) = \begin{cases} 1 - \lambda & \text{if } k = 0, \\ \lambda & \text{if } k = 1. \end{cases}$$

- Then, the user forms the query $\mathbf{Q} = (K, \mathbf{Q}_K)$ and sends it to the server, thus explicitly notifying which of the schemes, \mathcal{C}_0 or \mathcal{C}_1 , is used.
- Finally, the server replies according to \mathcal{C}_K using the query \mathbf{Q}_K .⁸

The leakage of \mathcal{C}_λ becomes

$$\begin{aligned} \rho(P_{\mathbf{Q}|M}) &= \rho(\lambda P_{\mathbf{Q}_1|M} + (1-\lambda)P_{\mathbf{Q}_0|M}) \\ &\stackrel{(a)}{\leq} \lambda \rho(P_{\mathbf{Q}_1|M}) + (1-\lambda)\rho(P_{\mathbf{Q}_0|M}) \\ &= \lambda L_1 + (1-\lambda)L_0, \end{aligned}$$

where (a) holds because of the convexity of ρ .

The proof for the distortion and the rate follows in a similar manner (they are not just convex but also linear). Hence, the set of achievable rate-distortion-leakage triples constitutes a convex set.

APPENDIX B PROOF OF THEOREM 1

Convexity. We prove the convexity for $R(D, L)$ based on the assumption that $\rho(P_{\mathbf{Q}|M})$ is convex in $P_{\mathbf{Q}|M}$, i.e., we have

$$\begin{aligned} L_\lambda &\triangleq \rho(\lambda P_{\mathbf{Q}_1|M} + (1-\lambda)P_{\mathbf{Q}_0|M}) \\ &\leq \lambda \rho(P_{\mathbf{Q}_1|M}) + (1-\lambda)\rho(P_{\mathbf{Q}_0|M}) \leq \lambda L_1 + (1-\lambda)L_0, \end{aligned}$$

for $0 \leq \lambda \leq 1$, where $\rho(P_{\mathbf{Q}_0|M}) \leq L_0$ and $\rho(P_{\mathbf{Q}_1|M}) \leq L_1$. Note that since the queries should be generated without knowing any realizations of the retrieved files, it is quite natural to have $I(X^{[M]}; \mathbf{Q}) = 0$. Thus, the objective function in the minimization of (10) can be expressed as

$$\begin{aligned} I(X^{[M]}; \hat{X}^{[M]} | \mathbf{Q}) &= I(X^{[M]}; \hat{X}^{[M]} | \mathbf{Q}) + \underbrace{I(X^{[M]}; \mathbf{Q})}_{=0} \\ &= I(X^{[M]}; \hat{X}^{[M]}, \mathbf{Q}). \end{aligned}$$

Now, let the distributions $P_{\hat{X}_1^{[M]}, \mathbf{Q}_1 | X^{[M]}}$ and $P_{\hat{X}_0^{[M]}, \mathbf{Q}_0 | X^{[M]}}$ achieve $R(D_1, L_1)$ and $R(D_0, L_0)$, respectively. Given $P_{\hat{X}_\lambda^{[M]}, \mathbf{Q}_\lambda | X^{[M]}} \triangleq \lambda P_{\hat{X}_1^{[M]}, \mathbf{Q}_1 | X^{[M]}} + (1-\lambda)P_{\hat{X}_0^{[M]}, \mathbf{Q}_0 | X^{[M]}}$ for any $0 \leq \lambda \leq 1$, using the convexity of MI in $P_{\hat{X}^{[M]}, \mathbf{Q} | X^{[M]}}$ we obtain

$$\begin{aligned} I(X^{[M]}; \hat{X}_\lambda^{[M]}, \mathbf{Q}_\lambda) \\ \leq \lambda I(X^{[M]}; \hat{X}_1^{[M]}, \mathbf{Q}_1) + (1-\lambda)I(X^{[M]}; \hat{X}_0^{[M]}, \mathbf{Q}_0). \end{aligned} \quad (12)$$

Further, one can also see that $P_{\mathbf{Q}_\lambda|M} = \lambda P_{\mathbf{Q}_1|M} + (1-\lambda)P_{\mathbf{Q}_0|M}$ and $P_{\hat{X}_\lambda^{[M]}|X^{[M]}} = \lambda P_{\hat{X}_1^{[M]}|X^{[M]}} + (1-\lambda)P_{\hat{X}_0^{[M]}|X^{[M]}}$. From the convexity of $\rho(\cdot)$ and the linearity of the distortion, it is straightforward to see that $\lambda L_1 + (1-\lambda)L_0 \geq L_\lambda$ and $\lambda D_1 + (1-\lambda)D_0 \geq D_\lambda$. Hence, from the definition of $R(D, L)$ we get

$$\begin{aligned} R(\lambda D_1 + (1-\lambda)D_0, \lambda L_1 + (1-\lambda)L_0) \\ &\stackrel{(a)}{\leq} R(D_\lambda, L_\lambda) \leq I(X^{[M]}; \hat{X}_\lambda^{[M]}, \mathbf{Q}_\lambda) \\ &\stackrel{(b)}{\leq} \lambda R(D_1, L_1) + (1-\lambda)R(D_0, L_0). \end{aligned}$$

⁸Formally, the scheme \mathcal{C}_1 is now using queries of the form $(1, \mathbf{Q}_1)$, but a constant prefix does not change the distribution and, thus, the leakage. The same holds for \mathcal{C}_0 .

where (a) holds since the minimization is taken over a smaller constrained set, and (b) follows from (12). This then completes the proof of convexity of $R(D, L)$.

In the following, we show that for the case of memoryless vector sources $\mathbf{X}^{[M]}$, the converse bound for the achievable rate R is indeed $R(D, L)$.

Consider an i.i.d. sequence $\{X_i^{[M]}\}_{i=1}^\beta = \{X_i^{(1)}, \dots, X_i^{(M)}\}_{i=1}^\beta$, where each element $X_i^{[M]}$ is distributed according to a prototype PMF $P_{X^{(1)}, \dots, X^{(M)}}$. The answer encoder f_A takes the input sequence $\{X_i^{[M]}\}_{i=1}^\beta$ and the generated query \mathbf{Q} to construct the codewords that are indexed by $\mathcal{A} = \{1, 2, \dots, 2^{\beta R}\}$. The reconstruction decoder $f_{\hat{X}}$ outputs an estimate $\{\hat{X}_i^{[M]}\}_{i=1}^\beta$ for $\hat{X}_i^{[M]} = \{\hat{X}_i^{(m)}\}_{m=1}^M$ using the answer \mathbf{A} ,⁹ requested index M , and the generated query \mathbf{Q} at the user side. A feasible scheme should satisfy

$$\frac{1}{\beta} \sum_{i=1}^\beta \mathbb{E}_{M, \mathbf{Q}, \mathbf{X}^{[M]}} \left[d_i(X_i^{(M)}, \hat{X}_i^{(M)}) \right] \leq D, \quad \rho(P_{\mathbf{Q}|M}) \leq L.$$

Hence, using the fact that the average code length over a source code is bounded from below by the entropy of the source, e.g., see [44, Thm. 5.4.1], we have

$$\begin{aligned} \beta R &\geq H(\mathbf{A} | \mathbf{Q}) \\ &\stackrel{(a)}{=} H(\mathbf{A} | \mathbf{Q}) - H(\mathbf{A} | \{X_i^{[M]}\}_{i=1}^\beta, \mathbf{Q}) \\ &= I(\{X_i^{[M]}\}_{i=1}^\beta; \mathbf{A} | \mathbf{Q}) \\ &\stackrel{(b)}{\geq} I(\{X_i^{[M]}\}_{i=1}^\beta; \{\hat{X}_i^{[M]}\}_{i=1}^\beta | \mathbf{Q}) \\ &\stackrel{(c)}{\geq} \sum_{i=1}^\beta H(X_i^{[M]} | \mathbf{Q}) - \sum_{i=1}^\beta H(X_i^{[M]} | \hat{X}_i^{[M]}, \mathbf{Q}) \\ &= \sum_{i=1}^\beta I(X_i^{[M]}; \hat{X}_i^{[M]} | \mathbf{Q}), \\ &\stackrel{(d)}{\geq} \sum_{i=1}^\beta R\left(\mathbb{E}_{M, \mathbf{Q}, \mathbf{X}^{[M]}} \left[d_i(X_i^{(M)}, \hat{X}_i^{(M)}) \right], \rho(P_{\mathbf{Q}|M})\right) \\ &\stackrel{(e)}{\geq} \beta R \left(\frac{1}{\beta} \sum_{i=1}^\beta \mathbb{E}_{M, \mathbf{Q}, \mathbf{X}^{[M]}} \left[d_i(X_i^{(M)}, \hat{X}_i^{(M)}) \right], \rho(P_{\mathbf{Q}|M}) \right) \\ &\stackrel{(f)}{\geq} \beta R(D, L), \end{aligned}$$

where (a) holds since the answer \mathbf{A} is a function of $\{X_i^{[M]}\}_{i=1}^\beta$ and \mathbf{Q} ; (b) follows by the data processing inequality; (c) can be verified by using the chain rule of entropy and the fact that conditioning reduces entropy; (d) is from the definition of $R(D, L)$ in (10) and the fact that all d_i are equal; (e) holds because $R(D, L)$ is convex; and (f) is from the fact that $R(D, L)$ is nonincreasing and $1/\beta \sum_{i=1}^\beta \mathbb{E}_{M, \mathbf{Q}, \mathbf{X}^{[M]}} \left[d_i(X_i^{(M)}, \hat{X}_i^{(M)}) \right] \leq D$, $\rho(P_{\mathbf{Q}|M}) \leq L$. Hence, for any scheme that satisfies the distortion constraint $\mathbb{E}_{M, \mathbf{Q}, \mathbf{X}^{[M]}} \left[d(\mathbf{X}^{(M)}, \hat{\mathbf{X}}^{(M)}) \right] \leq D$ and the leakage constraint $\rho(P_{\mathbf{Q}|M}) \leq L$, the rate should be larger than or equal to $R(D, L)$. This completes the converse proof.

⁹Here, without loss of generality, we assume that the reconstruction, denoted by $\hat{\mathbf{X}}^{[M]}$, has the same dimensions as $\mathbf{X}^{[M]}$. However, the user can choose the desired file $\mathbf{X}^{(M)}$ to retrieve, i.e., the M -th entry of $\hat{\mathbf{X}}^{[M]}$.

APPENDIX C

ACHIEVABLE SCHEMES FROM SECTION III-C

A. Compression-Based Scheme for Gaussian Data

As a reference for synthetic Gaussian data (see Fig. 3(a)), we used the compression-based scheme outlined in Section III-C. As explained in Section III-C, the scheme reduces to quantization of random vectors drawn from an $N\beta$ -dimensional multivariate Gaussian distribution for $N = 1, 2, \dots, M$ and different numbers of quantization vectors (i.e., different rates). We used the generalized Lloyd algorithm, also known as the Linde-Buzo-Gray (or LBG) algorithm [20], [21]. Note that this algorithm is closely related to k -means clustering in unsupervised learning [57]. The authors argue in [21] that although their approach is not guaranteed to provide the best quantizer, its results are nearly optimal for a wide class of distributions.

We briefly explain the steps of finding the quantization vectors (or levels) below and refer the interested reader to [21] for further details. When quantizing a Gaussian vector into r bits, the number of quantization vectors is $k = 2^r$. For each N , we modify the original Gaussian training dataset with n samples, described in Section V, into a dataset of size $m = \binom{M}{N}n$ by first shifting each file by its sample mean (to ensure the same distribution for each file) and then generating all N -subsets of M files for each sample.¹⁰ The resulting dataset $\{z(l) = (z^{(1)}(l), \dots, z^{(N)}(l))\}_{l=1}^m$ of $N\beta$ -dimensional vectors is used to find quantization vectors as follows.

- 1) Randomly select an initial set of quantization vectors $\{q_j = (q_j^{(1)}, \dots, q_j^{(N)})\}_{j=1}^k$.
- 2) Continue iterating as follows.
 - a) Each sample vector $z(l)$ is quantized to (approximated by) its closest quantization vector (its “nearest neighbor”) $q_{j^*(l)}$, where $j^*(l) = \arg \min_j \frac{1}{N} \sum_{i=1}^N d(z^{(i)}(l), q_j^{(i)})$. This gives a mean quantization error (or distortion) among all the sample vectors of $D = \frac{1}{(m \cdot N)} \sum_{l=1}^m \sum_{i=1}^N d(z^{(i)}(l), q_{j^*(l)}^{(i)})$.
 - b) Each quantization vector is updated to the mean of the sample vectors as $q_j \leftarrow \frac{1}{|Z_j|} \sum_{z \in Z_j} z$, where the set of sample vectors that are quantized to q_j is denoted by Z_j (“neighborhood” of q_j).
- 3) The algorithm stops when the mean quantization error between two consecutive iterations changes less than a predefined threshold.

Since the mean quantization error (or distortion) D is non-negative and nonincreasing between iterations, the algorithm is guaranteed to converge. Since it is a randomized algorithm, we ran it multiple times and chose the quantizer that produced the smallest mean quantization error. Obtained quantization vectors are tested on the test dataset, shifted by the sample mean of the training dataset. As a final remark, we remind the reader that our goal here is not to find the best quantization possible, but only to have a good enough approximation.

¹⁰This shifting is without loss of generality since the distortion function $d(\cdot, \cdot)$ is translation invariant.

Additionally, after the achievable points are calculated, we make sure they all satisfy the convexity property (cf. Lemma 1). More precisely, if the triples (R_0, D_0, L_0) , (R_1, D_1, L_1) , and $(\lambda R_1 + (1 - \lambda)R_0, D_2, \lambda L_1 + (1 - \lambda)L_0)$ are achievable for some $0 < \lambda < 1$, we update $D_2 \leftarrow \min(D_2, \lambda D_1 + (1 - \lambda)D_0)$.

B. Shannon’s Scheme for Gaussian Data

This section briefly outlines Shannon’s scheme for Gaussian data (plotted in Fig. 3(a)). Following its description in Section III-C, the server compresses N , $N \in [M]$, independent files, each consisting of β independent Gaussian RVs, together. It is known from the rate-distortion theory for multi-dimensional sources [47], as the file size $\beta \rightarrow \infty$, that a download rate $R = NR_G(D)$ is achievable with distortion D . Here, $R_G(D) = \max\{\frac{1}{2} \log(\sigma^2/D), 0\}$ for a Gaussian RV distributed according to $\mathcal{N}(\mu, \sigma^2)$ [44, Ch. 10]. Similar to Appendix C-A, we further use a convexifying approach to obtain an achievable scheme for any hard decision leakage (or accuracy) $1/M \leq L \leq 1$. In the following, we brief describe the scheme. First, we select two accuracy values, say L_0 and L_1 , $L_0, L_1 \in \{1, 1/2, \dots, 1/M\}$. Applying the Gaussian rate-distortion function of $R_G(D) = \frac{1}{2} \log(\sigma^2/D)$, $D \in (0, \sigma^2]$, to the previously outlined scheme, one can obtain two achievable distortions $D_G(R_0, L_0) = \sigma^2 \cdot 2^{-2R_0 L_0}$ and $D_G(R_1, L_1) = \sigma^2 \cdot 2^{-2R_1 L_1}$. Next, the desired accuracy $L \in [L_0, L_1]$ is selected to be $L = \lambda L_1 + (1 - \lambda)L_0$, and the goal is to determine the minimum possible linear combination of $D_G(R_0, L_0)$ and $D_G(R_1, L_1)$ subject to $R = \lambda R_1 + (1 - \lambda)R_0$, i.e.,

$$\min_{\substack{L_0^{-1}, L_1^{-1} \in [M] \\ L = \lambda L_1 + (1 - \lambda)L_0}} \min_{R = \lambda R_1 + (1 - \lambda)R_0} [\lambda D_G(R_1, L_1) + (1 - \lambda)D_G(R_0, L_0)]. \quad (13)$$

This then gives the performance of the synthetic Gaussian dataset in Fig. 3(a). As a final remark, we also numerically evaluate the values of $R(D, L)$ for the Gaussian dataset. For instance, for $D = 1.875$ and $L = 0.6$, we obtain $R(D, L) \approx 2.035$, while (13) gives 1.875 for $(R, L) = (2.0, 0.6)$, confirming that our proposed Shannon’s scheme performs very close to the information-theoretical optimum.

C. Compression-Based Scheme for the MNIST Dataset

The scheme is based on the ideas of Section III-C and reduces to choosing a lossy compression method for a single image (a single compressor for all digits is considered). First, we applied a grayscale compression similar to the instruments used by the JPEG standard. We refer the interested reader to [52, Sec. 8.2] for more details and other techniques for image compression. The main ingredient of the JPEG standard is a two-dimensional discrete cosine transform. In the standard, an image is split into 8×8 blocks and the transform is applied to each block independently. Since the images from the MNIST dataset are of size 28×28 , we applied the transform to 7×7 blocks. In this way, an image is split into 16 blocks. Next, the resulting values were quantized by a uniform scalar

TABLE IV

NEURAL NETWORK (NN) ARCHITECTURES USED FOR TRAINING FOR THE SYNTHETIC GAUSSIAN DATASET. FC STANDS FOR A FULLY CONNECTED LAYER. SIZE IS THE NUMBER OF NEURONS OR INPUT SIZE. AS ACTIVATION FUNCTION WE USED THE SCALED EXPONENTIAL LINEAR UNIT (SELU) [58], SOFTMAX, AND SIGMOID. WE ADDED A SKIP CONNECTION BETWEEN THE FIRST LAYER AND THE FOURTH LAYER OF THE QUERY GENERATOR NETWORK TO IMPROVE THE GRADIENT PROPAGATION FOR THE TRAINING [59].

NN	Detailed architecture (consecutive layers' sizes and types)
Query generator, f_Q	8 (Input), 8 (FC, SeLU), 8 (FC, SeLU), 8 (FC, SeLU), 8 (FC, SeLU), 4 (FC, SeLU)
Answer generation, f_A	$4 + 3 \times 4 \times 1$ (Input), 16 (Flatten), 256 (FC, SeLU), 256 (FC, SeLU), 256 (FC, SeLU), 256 (FC, SeLU), 256 (FC, SeLU), 256 (FC, SeLU), 256 (FC, SeLU), 256 (FC, SeLU), Answer dim (FC, sigmoid)
Decoder, $f_{\hat{X}}$	Answer dim + 8 (Input), 256 (FC, SeLU), 256 (FC, SeLU), 256 (FC, SeLU), 256 (FC, SeLU), 256 (FC, SeLU), 256 (FC, SeLU), 256 (FC, SeLU), 256 (FC, SeLU), 256 (FC, SeLU), 256 (FC, SeLU), 3 (FC)
Adversary, $f_{\hat{M}}$	4 (Input), 64 (FC, SeLU), 64 (FC, SeLU), 64 (FC, SeLU), 64 (FC, SeLU), 64 (FC, SeLU), 64 (FC, SeLU), 64 (FC, SeLU), 4 (FC, softmax)

quantizer. For each block, the top-left coefficients play the most important role as they grasp the low-frequency contents of the block. Thus, they are assigned more bits from the available pool of bits (defined by the desired rate). Finally, these quantized coefficients were encoded with a combination of run-length encoding and a two-dimensional Huffman code.

Since the MNIST images have a small size, the entropy coding techniques do not provide any compression benefits. For example, the usually ignored overhead of storing the Huffman coding table requires too many bits in our case. Also, the run-length encoder performs poorly as there are not many repetitive values, increasing the size of an MNIST image on many occasions. Therefore, we turned to a much simpler scalar quantization of the original grayscale images.

Let us describe this method in more details. Assume we split a 28×28 pixels image into rectangular blocks of the same size $h \times w$ each and all values in each block are substituted by the mean value of the block forming one large “pixel”. If we allocate r bits to storing these mean values, each of them can be quantized to 2^r quantization points on $[0, 255]$ either uniformly (U) or nonuniformly (NU) spread. Such a scheme requires $28/h \cdot 28/w \cdot r$ bits for encoding one image and thus has a rate of r/hw bits per pixel. The distortion of the scheme is explicitly calculated from compressing and decompressing the training subset of the MNIST dataset. We exhaustively checked all choices of h , w , r , and for each choice optimized the locations of the quantization points (in the NU case) using the generalized Lloyd algorithm in order to find the best ones for each target value of the required rate. The obtained sets of parameters were further tested on the test subset of the MNIST dataset.

D. Compression-Based Scheme for the CIFAR-10 and LSUN Datasets

The compression-based scheme for CIFAR-10 and LSUN is rather similar to the scheme for MNIST, considering a single compressor for all classes compressing a single image. The only difference being a standard image preprocessing stage that is very common when compressing color images. First, the image is transformed from red, green, and blue channel representation to luminance-chrominance representation, consisting of brightness, hue, and saturation channels. Next, the hue and saturation channels are decimated by a factor of 2. In other words, four neighboring pixels that form a 2×2 block are described by four values of brightness, one value of hue, and

one value of saturation. These channels are further quantized in a similar manner as for MNIST. However, nonuniform quantization showed to give no improvements for the CIFAR-10 and LSUN datasets (and often is actually worse than uniform quantization). We believe this is because of a much more diverse space of images in these datasets (as opposed to MNIST) and thus, fitting quantization points to the training datasets' block distributions has a negative effect on the rate-distortion curves, when calculated on the test subsets of the datasets. We thus do not present the results of nonuniform quantization.

APPENDIX D

LEARNING FOR THE DATA-DRIVEN APPROACH

As elaborated in Section IV-A, the learning is done by implementing the iterative algorithm of Algorithm 1. Here, the learning rate is selected empirically for each accuracy and distortion level with the RMSprop optimizer, and the number of iterations T is selected empirically and individually for each dataset and training point. The number of training samples, denoted by n , for the Gaussian case is set to 1000000 (250000 for each of the $M = 4$ files) and to 60000 (6000 for each digit), 50000 (5000 for each class), and 1200000 (120000 for each class) for the MNIST, CIFAR-10, and LSUN datasets, respectively. For the image datasets, we used a minibatch size of $b = 32$, while for the synthetic Gaussian dataset, we used a minibatch size of $b = 2048$.

The architectures of the deep neural networks representing the functions f_Q , f_A , $f_{\hat{X}}$, and $f_{\hat{M}}$ used for training for the synthetic Gaussian dataset are detailed in Table IV. In the special case of accuracy $L = 1$, i.e., full leakage, the problem reduces to the classical rate-distortion problem, and to improve performance, we only considered an encoder (for compression of the requested file), corresponding to f_A , and a decoder (for decompression at the user side), corresponding to $f_{\hat{X}}$. Both the encoder and the decoder are represented as deep neural networks and trained in the classical way [60] (due to space limitations, the actual architectures are not tabulated).

For the MNIST dataset there are $M = 10$ files (there are 10 digits) and each file is of size $\beta = 28 \times 28 = 784$ symbols, or $784 \times 8 = 6272$ bits (each picture is of size 28×28 pixels and each pixel is of size 8 bits). For the CIFAR-10 dataset, there are also $M = 10$ files (there are 10 classes of files) and each file is of size $\beta = 32 \times 32 = 1024$ symbols, or $1024 \times 8 \times 3 = 24576$ bits (each picture is of size 32×32

TABLE V

NEURAL NETWORK ARCHITECTURES USED FOR TRAINING FOR THE IMAGE DATASETS. THE INPUT PIXEL VALUE IS RESCALED BETWEEN -1.0 AND 1.0 . FC STANDS FOR A FULLY CONNECTED LAYER. CONV AND CONV^T STAND FOR A CONVOLUTIONAL AND A TRANSPOSED CONVOLUTIONAL LAYER, RESPECTIVELY, AND “ST” IS SHORTHAND FOR STRIDE. SIZE IS THE NUMBER OF NEURONS OR INPUT SIZE. AS ACTIVATION FUNCTION WE USED SELU, HYPERBOLIC TANGENT (TANH), SOFTMAX, AND SIGMOID. WE ADDED A SKIP CONNECTION BETWEEN THE FIRST LAYER AND THE FOURTH LAYER OF THE QUERY GENERATOR NETWORK TO IMPROVE THE GRADIENT PROPAGATION FOR THE TRAINING [59].

NN	Detailed architecture (consecutive layers’ sizes and types)
Same for all datasets	
Query generator, f_Q	20 (Input), 20 (FC, SeLU), 20 (FC, SeLU), 20 (FC, SeLU), 9 (FC, SeLU), 7 (FC, SeLU), 5 (FC, SeLU)
Answer generation part 1, f_A	5 (Input), 5 (FC, SeLU), 7 (FC, SeLU), 9 (FC, SeLU), 10 (FC, softmax)
Adversary, f_M	5 (Input), 64 (FC, SeLU), 64 (FC, SeLU), 64 (FC, SeLU), 64 (FC, SeLU), 64 (FC, SeLU), 64 (FC, SeLU), 10 (FC, softmax)
MNIST dataset	
Answer generation part 2, f_A	$10 \times 28 \times 28 \times 1$ (Input), $10 \times 26 \times 26 \times 8$ (Conv, SeLU), $10 \times 12 \times 12 \times 8$ (Conv (st = 2), SeLU), $10 \times 10 \times 10 \times 16$ (Conv, SeLU), $10 \times 4 \times 4 \times 16$ (Conv (st = 2), SeLU), 256×10 (Concatenate 10 parallel outputs of previous layers)
Answer generation part 3, f_A	$10 + 256 \times 10$ (Input), 256×10 (Broadcast and elementwise multiply), 2560 (Flatten), 5 (Input), 2048 (FC, SeLU), 1024 (FC, SeLU), Answer dim (FC, sigmoid)
Decoder, $f_{\hat{X}}$	Answer dim + 20 (Input), 512 (FC, SeLU), 512 (FC, SeLU), 512 (FC, SeLU), $4 \times 4 \times 32$ (Unflatten), $11 \times 11 \times 64$ (ConvT (st = 2), SeLU), $25 \times 25 \times 128$ (ConvT (st = 2), SeLU), $28 \times 28 \times 1$ (ConvT (st = 2), tanh)
CIFAR-10 and LSUN datasets, 32×32 pixels images	
Answer generation part 2, f_A	$10 \times 32 \times 32 \times 3$ (Input), $10 \times 30 \times 30 \times 8$ (Conv, SeLU), $10 \times 14 \times 14 \times 8$ (Conv (st = 2), SeLU), $10 \times 12 \times 12 \times 16$ (Conv, SeLU), 2304×10 (Concatenate 10 parallel outputs of previous layers)
Answer generation part 3, f_A	$10 + 2304 \times 10$ (Input), 2304×10 (Broadcast and elementwise multiply), 23040 (Flatten), 5 (Input), 2304 (FC, SeLU), 1024 (FC, SeLU), Answer dim (FC, sigmoid)
Decoder, $f_{\hat{X}}$	Answer dim + 20 (Input), 512 (FC, SeLU), 512 (FC, SeLU), 512 (FC, SeLU), $4 \times 4 \times 32$ (Unflatten), $8 \times 8 \times 16$ (ConvT (st = 2), SeLU), $16 \times 16 \times 8$ (ConvT (st = 2), SeLU), $32 \times 32 \times 3$ (ConvT (st = 2), tanh)
LSUN dataset, 64×64 pixels images	
Answer generation part 2, f_A	$10 \times 64 \times 64 \times 3$ (Input), $10 \times 62 \times 62 \times 128$ (Conv, SeLU), $10 \times 60 \times 60 \times 128$ (Conv, SeLU), $10 \times 29 \times 29 \times 128$ (Conv (st = 2), SeLU), $10 \times 27 \times 27 \times 256$ (Conv, SeLU), $10 \times 25 \times 25 \times 256$ (Conv, SeLU), $10 \times 12 \times 12 \times 256$ (Conv (st = 2), SeLU), $10 \times 10 \times 10 \times 512$ (Conv, SeLU), $10 \times 4 \times 4 \times 96$ (Conv (st = 2), SeLU), 1536×10 (Concatenate 10 parallel outputs of previous layers)
Answer generation part 3, f_A	$10 + 1536 \times 10$ (Input), 1536×10 (Broadcast and elementwise multiply), 1536×2 (1×1 Conv), $16 \times 96 \times 2$ (Permutation and reshape), 3072 (Flatten), 5 (Input), 3072 (FC, SeLU), 1024 (FC, SeLU), 768 (FC, SeLU), 768×1 (Reshape), 768×2 (1×1 Conv, SeLU), 768×4 (1×1 Conv, sigmoid), Answer dim (Flatten)
Decoder, $f_{\hat{X}}$	Answer dim (Input), 768×4 (Reshape), 768×1 (1×1 Conv, SeLU), 768 (Flatten), 20 (Input), 768 (FC, SeLU), $4 \times 4 \times 48$ (Unflatten), $10 \times 10 \times 1024$ (ConvT (st = 2), SeLU), $8 \times 8 \times 512$ (Conv, SeLU), $18 \times 18 \times 256$ (ConvT (st = 2), SeLU), $16 \times 16 \times 256$ (Conv, SeLU), $34 \times 34 \times 128$ (ConvT (st = 2), SeLU), $70 \times 70 \times 64$ (ConvT (st = 2), SeLU), $68 \times 68 \times 64$ (Conv, SeLU), $66 \times 66 \times 64$ (Conv, SeLU), $64 \times 64 \times 3$ (ConvT (st = 2), tanh)

pixels and each pixel is of size 8 bits for each of the 3 color channels). For the LSUN dataset, there are $M = 10$ files and we consider two file sizes: one with images of size 32×32 pixels (for the data-driven approach with image splitting), and the other one with file size $\beta = 64 \times 64 = 4096$ symbols. The architectures of the deep neural networks representing the functions f_Q , f_A , $f_{\hat{X}}$, and f_M for the MNIST dataset, the CIFAR-10 and LSUN datasets with images of size 32×32 pixels, and the LSUN dataset with images of size 64×64 pixels are all given in Table V. Note that in contrast to the Gaussian case, in Table V we list descriptions of three neural networks for the answer function f_A , labeled as part 1 to 3. To produce the final answer, the output of the first network is fed to the third network together with the output from the second network and the queries (which are fed into the fourth/sixth layer of the network). The input to the first network is the queries, while the input to the second network is the set of files. The second network takes the set of files as input and extracts their features. Note that for the LSUN dataset with 64×64 pixels images, the input to the query network is fed into the fifth layer of the decoder network, while for the other datasets it is fed into the first layer. As for the Gaussian case, training for MNIST, CIFAR-10, and LSUN can be simplified for $L = 1$ as described above (again due to space limitations,

the actual architectures are not tabulated).

REFERENCES

- [1] B. Chor, O. Goldreich, E. Kushilevitz, and M. Sudan, “Private information retrieval,” in *Proc. 36th Annu. IEEE Symp. Found. Comp. Sci. (FOCS)*, Milwaukee, WI, USA, Oct. 23–25, 1995, pp. 41–50.
- [2] K. Banawan and S. Ulukus, “The capacity of private information retrieval from coded databases,” *IEEE Trans. Inf. Theory*, vol. 64, no. 3, pp. 1945–1956, Mar. 2018.
- [3] R. Freij-Hollanti, O. W. Gnilke, C. Hollanti, and D. A. Karpuk, “Private information retrieval from coded databases with colluding servers,” *SIAM J. Appl. Algebra Geom.*, vol. 1, no. 1, pp. 647–664, Nov. 2017.
- [4] S. Kopparty, S. Saraf, and S. Yekhanin, “High-rate codes with sublinear-time decoding,” in *Proc. 43rd Annu. ACM Symp. Theory Comput. (STOC)*, San Jose, CA, USA, Jun. 6–8, 2011, pp. 167–176.
- [5] H. Sun and S. A. Jafar, “The capacity of private information retrieval,” *IEEE Trans. Inf. Theory*, vol. 63, no. 7, pp. 4075–4088, Jul. 2017.
- [6] R. Tajeddine, O. W. Gnilke, and S. El Rouayheb, “Private information retrieval from MDS coded data in distributed storage systems,” *IEEE Trans. Inf. Theory*, vol. 64, no. 11, pp. 7081–7093, Nov. 2018.
- [7] S. Yekhanin, “Private information retrieval,” *Commun. ACM*, vol. 53, no. 4, pp. 68–73, Apr. 2010.
- [8] H.-Y. Lin, S. Kumar, E. Rosnes, A. Graell i Amat, and E. Yaakobi, “Multi-server weakly-private information retrieval,” *IEEE Trans. Inf. Theory*, vol. 68, no. 2, pp. 1197–1219, Feb. 2022.
- [9] —, “The capacity of single-server weakly-private information retrieval,” *IEEE J. Sel. Areas Inf. Theory*, vol. 2, no. 1, pp. 415–427, Mar. 2021.
- [10] I. Samy, M. Attia, R. Tandon, and L. Lazos, “Asymmetric leaky private information retrieval,” *IEEE Trans. Inf. Theory*, vol. 67, no. 8, pp. 5352–5369, Aug. 2021.

- [11] R. Zhou, T. Guo, and C. Tian, "Weakly private information retrieval under the maximal leakage metric," in *Proc. IEEE Int. Symp. Inf. Theory (ISIT)*, Los Angeles, CA, USA, Jun. 21–26, 2020, pp. 1089–1094.
- [12] C. Qian, R. Zhou, C. Tian, and T. Liu, "Improved weakly private information retrieval codes," in *Proc. IEEE Int. Symp. Inf. Theory (ISIT)*, Espoo, Finland, Jun. 26–Jul. 1, 2022, pp. 2840–2845.
- [13] R. R. Toledo, G. Danezis, and I. Goldberg, "Lower-cost ϵ -private information retrieval," in *Proc. Privacy Enhancing Technol. Symp. (PETS)*, Darmstadt, Germany, Jul. 19–22, 2016, pp. 184–201.
- [14] I. J. Goodfellow, J. Pouget-Abadie, M. Mirza, B. Xu, D. Warde-Farley, S. Ozair, A. Courville, and Y. Bengio, "Generative adversarial nets," in *Proc. 28th Int. Conf. Neural Inf. Process. Syst. (NeurIPS)*, Montréal, QC, Canada, Dec. 8–13, 2014, pp. 2672–2680.
- [15] J. T. Springenberg, "Unsupervised and semi-supervised learning with categorical generative adversarial networks," in *Proc. Int. Conf. Learn. Representations (ICLR)*, San Juan, Puerto Rico, May 2–4, 2016.
- [16] A. Odena, C. Olah, and J. Shlens, "Conditional image synthesis with auxiliary classifier GANs," in *Proc. Int. Conf. Mach. Learn. (ICML)*, Sydney, Australia, Aug. 6–11, 2017, pp. 2642–2651.
- [17] Y. LeCun, L. Bottou, Y. Bengio, and P. Haffner, "Gradient-based learning applied to document recognition," *Proc. IEEE*, vol. 86, no. 11, pp. 2278–2324, Nov. 1998.
- [18] A. Krizhevsky, "Learning multiple layers of features from tiny images," University of Toronto, Tech. Rep., Apr. 2009.
- [19] F. Yu, A. Seff, Y. Zhang, S. Song, T. Funkhouser, and J. Xiao, "LSUN: Construction of a large-scale image dataset using deep learning with humans in the loop," Jun. 2015, arXiv:1506.03365v3 [cs.CV].
- [20] S. P. Lloyd, "Least squares quantization in PCM," *IEEE Trans. Inf. Theory*, vol. 28, no. 2, pp. 129–137, Mar. 1982.
- [21] Y. Linde, A. Buzo, and R. M. Gray, "An algorithm for vector quantizer design," *IEEE Trans. Commun.*, vol. 28, no. 1, pp. 84–95, Jan. 1980.
- [22] R. Baeza-Yates and B. Ribeiro-Neto, *Modern Information Retrieval*. Boston, MA, USA: Addison-Wesley, 1999.
- [23] J. Wang, L. Yu, W. Zhang, Y. Gong, Y. Xu, B. Wang, P. Zhang, and D. Zhang, "IRGAN: A minimax game for unifying generative and discriminative information retrieval models," in *Proc. 40th Int. ACM Conf. Res. Develop. Inf. Retrieval (SIGIR)*, Shinjuku, Tokyo, Japan, Aug. 7–11, 2017, pp. 515–524.
- [24] D. Kifer and A. Machanavajjhala, "No free lunch in data privacy," in *Proc. ACM SIGMOD Int. Conf. Manage. Data (SIGMOD)*, Athens, Greece, Jun. 12–16, 2011, pp. 193–204.
- [25] C. Dwork, F. McSherry, K. Nissim, and A. Smith, "Calibrating noise to sensitivity in private data analysis," in *Proc. Theory Cryptography Conf. (TCC)*, New York, NY, USA, Mar. 4–7, 2006, pp. 265–284.
- [26] C. Dwork, "Differential privacy," in *Proc. 33rd Int. Coll. Automata, Lang. Program. (ICALP), part II*, Venice, Italy, Jul. 10–14, 2006, pp. 1–12.
- [27] M. Seif, R. Tandon, and M. Li, "Context aware Laplacian mechanism for local information privacy," in *Proc. IEEE Inf. Theory Workshop (ITW)*, Visby, Sweden, Aug. 25–28, 2019.
- [28] T. Stadler, B. Oprisanu, and C. Troncoso, "Synthetic data – Anonymisation groundhog day," in *Proc. 31st USENIX Secur. Symp.*, Boston, MA, USA, Aug. 10–12, 2022.
- [29] Y. Wang, S. Aeron, A. S. Rakin, T. Koike-Akino, and P. Moulin, "Robust machine learning via privacy/rate-distortion theory," in *Proc. IEEE Int. Symp. Inf. Theory (ISIT)*, Melbourne, Australia, Jul. 12–20, 2021, pp. 1320–1325.
- [30] C. Feutry, P. Piantanida, Y. Bengio, and P. Duhamel, "Learning anonymized representations with adversarial neural networks," Feb. 2018, arXiv:1802.09386v1 [stat.ML].
- [31] Z. Wu, Z. Wang, Z. Wang, and H. Jin, "Towards privacy-preserving visual recognition via adversarial training: A pilot study," in *Proc. Eur. Conf. Comput. Vision (ECCV)*, Munich, Germany, Sep. 8–14, 2018, pp. 627–645.
- [32] A. Li, J. Guo, H. Yang, F. D. Salim, and Y. Chen, "DeepObfuscator: Obfuscating intermediate representations with privacy-preserving adversarial learning on smartphones," in *Proc. ACM/IEEE Int. Conf. IoT Des. Implementation (IoTDI)*, Charlottesville, VA, USA, May 18–21, 2021, pp. 28–39.
- [33] C. Huang, P. Kairouz, X. Chen, L. Sankar, and R. Rajagopal, "Context-aware generative adversarial privacy," *Entropy*, vol. 19, no. 12, Dec. 2017.
- [34] —, "Generative adversarial privacy," in *ICML'18 Workshop: Privacy Mach. Learn. Artif. Intell. (PiMLAI)*, Stockholm, Sweden, Jul. 15, 2018.
- [35] A. Tripathy, Y. Wang, and P. Ishwar, "Privacy-preserving adversarial networks," in *Proc. 57th Allerton Conf. Commun., Control, Comput.*, Monticello, IL, USA, Sep. 24–27, 2019, pp. 495–505.
- [36] B.-W. Tseng and P.-Y. Wu, "Compressive privacy generative adversarial network," *IEEE Trans. Inf. Forens. Secur.*, vol. 15, pp. 2499–2513, 2020.
- [37] Y. Blau and T. Michaeli, "Rethinking lossy compression: The rate-distortion-perception tradeoff," in *Proc. Int. Conf. Mach. Learn. (ICML)*, Long Beach, CA, USA, Jun. 9–15, 2019, pp. 675–685.
- [38] E. Kushilevitz and R. Ostrovsky, "Replication is not needed: Single database, computationally-private information retrieval," in *Proc. 38th Annu. IEEE Symp. Found. Comp. Sci. (FOCS)*, Miami Beach, FL, USA, Oct. 20–22, 1997, pp. 364–373.
- [39] —, "One-way trapdoor permutations are sufficient for non-trivial single-server private information retrieval," in *Proc. 19th Annu. Int. Conf. Theory Appl. Crypto. Techn. (EUROCRYPT)*, Bruges, Belgium, May 14–18, 2000, pp. 104–121.
- [40] H. Lipmaa and K. Pavlyk, "A simpler rate-optimal CPIR protocol," in *Proc. 21st Int. Conf. Financial Crypto. Data Secur. (FC)*, Sliema, Malta, Apr. 3–7, 2017, pp. 621–638.
- [41] S. Kadhe, B. Garcia, A. Heidarzadeh, S. El Rouayheb, and A. Sprintson, "Private information retrieval with side information," *IEEE Trans. Inf. Theory*, vol. 66, no. 4, pp. 2032–2043, Apr. 2020.
- [42] I. Samy, M. A. Attia, R. Tandon, and L. Lazos, "Latent-variable private information retrieval," in *Proc. IEEE Int. Symp. Inf. Theory (ISIT)*, Los Angeles, CA, USA, Jun. 21–26, 2020, pp. 1071–1076.
- [43] S. Vithana, K. Banawan, and S. Ulukus, "Semantic private information retrieval," *IEEE Trans. Inf. Theory*, vol. 68, no. 4, pp. 2635–2652, Apr. 2022.
- [44] T. M. Cover and J. A. Thomas, *Elements of Information Theory*, 2nd ed. New York, NY, USA: Wiley, 2006.
- [45] T. T. Nguyen and S. Sanner, "Algorithms for direct 0-1 loss optimization in binary classification," in *Proc. Int. Conf. Mach. Learn. (ICML)*, Atlanta, GA, USA, Jun. 16–21, 2013, pp. 1085–1093.
- [46] A. D. Wyner and J. Ziv, "The rate-distortion function for source coding with side information at the decoder," *IEEE Trans. Inf. Theory*, vol. 22, no. 1, pp. 1–10, Jan. 1976.
- [47] R. M. Gray, "A new class of lower bounds to information rates of stationary sources via conditional rate-distortion functions," *IEEE Trans. Inf. Theory*, vol. 19, no. 4, pp. 480–489, Jul. 1973.
- [48] F. Mentzer, E. Agustsson, M. Tschannen, R. Timofte, and L. Van Gool, "Conditional probability models for deep image compression," in *Proc. IEEE/CVF Conf. Comput. Vision Pattern Recognit. (CVPR)*, Salt Lake City, UT, USA, Jun. 18–23, 2018, pp. 4394–4402.
- [49] J. Ballé, V. Laparra, and E. P. Simoncelli, "End-to-end optimized image compression," in *Proc. Int. Conf. Learn. Representations (ICLR)*, Toulon, France, Apr. 24–26, 2017.
- [50] Y. Yakimenka, H.-Y. Lin, E. Rosnes, and J. Kliewer, "Optimal rate-distortion-leakage tradeoff for single-server information retrieval," *IEEE J. Sel. Areas Commun.*, vol. 40, no. 3, pp. 832–846, Mar. 2022.
- [51] M. J. Sabin and R. M. Gray, "Global convergence and empirical consistency of the generalized Lloyd algorithm," *IEEE Trans. Inf. Theory*, vol. 32, no. 2, pp. 148–155, Mar. 1986.
- [52] I. Bocharova, *Compression for Multimedia*. Cambridge, U.K.: Cambridge University Press, 2010.
- [53] D. Salomon, *Data Compression: The Complete Reference*, 4th ed. New York, NY, USA: Springer, 2007.
- [54] I. Goodfellow, Y. Bengio, and A. Courville, *Deep Learning*. MIT Press, 2016. [Online]. Available: <http://www.deeplearningbook.org>
- [55] T. Salimans, I. Goodfellow, W. Zaremba, V. Cheung, A. Radford, and X. Chen, "Improved techniques for training GANs," in *Proc. 30th Int. Conf. Neural Inf. Process. Syst. (NeurIPS)*, Barcelona, Spain, Dec. 5–10, 2016, pp. 2234–2242.
- [56] I. Goodfellow, "NIPS 2016 tutorial: Generative adversarial networks," Jan. 2017, arXiv:1701.00160v4 [cs.LG].
- [57] C. Levrard, "Quantization/clustering: when and why does k -means work?" *J. French Statist. Soc.*, vol. 159, no. 1, pp. 1–26, 2018.
- [58] G. Klambauer, T. Unterthiner, A. Mayr, and S. Hochreiter, "Self-normalizing neural networks," in *Proc. 31th Int. Conf. Neural Inf. Process. Syst. (NeurIPS)*, Long Beach, CA, USA, Dec. 4–9, 2017, pp. 972–981.
- [59] K. He, X. Zhang, S. Ren, and J. Sun, "Deep residual learning for image recognition," in *Proc. IEEE/CVF Conf. Comput. Vision Pattern Recognit. (CVPR)*, Las Vegas, NV, USA, Jun. 26 – Jul. 1, 2016, pp. 770–778.
- [60] D. P. Kingma and M. Welling, "Auto-encoding variational Bayes," in *Proc. Int. Conf. Learn. Representations (ICLR)*, Banff, AB, Canada, Apr. 14–16, 2014.